ASSESSMENT OF GEOPHYSICAL FLOWS FOR ZERO-GRAVITY SIMULATION

FINAL REPORT

NAS8-31347

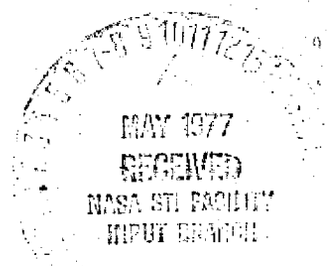

C. Byron Winn, Andrew Cox, and R. Srivatsangam

Department of Mechanical Engineering
Colorado State University
Fort Collins, Colorado 80523

December, 1976

C O N T E N T S

A B S T R A C T

The results of research relating to the feasibility of using a low gravity environment to model geophysical flows are presented in this report. Atmospheric and solid earth flows are considered. Possible experiments and their required apparatus are suggested.

INTRODUCTION

The advent of the space shuttle presents exciting possibilities for developing physical models of geophysical flow phenomena that cannot be adequately modeled in the earth's gravitational environment.

During the past decade significant advances in the development of theoretical models of geophysical phenomena have taken place. For example, the theory of new global tectonics has led to the development of many new mathematical models of the solid earth. These have had a significant bearing on the understanding of such important phenomena as earthquakes. In addition to the models associated with the solid earth, an atmospheric circulation model has also been recently developed. Many of the components of these models could be validated if a zero G environment were available.

It is known that dynamical processes in various parts of the earth are responsible for variations in the length of the day. These variations comprise three distinct components: (1) seasonal fluctuations on the order of 1×10^{-3} sec., (2) irregular decade fluctuations on the order of 5×10^{-3} sec., and (3) a secular increase in the length of the day by about 1×10^{-3} sec. per century. The secular increase is associated with angular momentum transfer of the earth to the moon caused by the action of gravitational torques associated with the tidal bulge. Seasonal fluctuations are caused by torques on the mantle produced by the combined effect of atmospheric winds and ocean currents. The amplitude of the decade fluctuations is too large to be accounted for in terms of interactions of the ocean and atmosphere and geophysicists generally agree that these fluctuations must therefore be due to angular momentum transfer between the mantle and the liquid core. The nature of the stresses that couple the core to the mantle must account for the fluctuating torques at the core mantle interface which are implied

by the decade fluctuations. The specific nature of these stresses cannot be determined without detailed theoretical calculations of specific models of the coupling process. In the past, symmetric models have typically been considered but there now exists substantial and growing evidence--to which satellite observations have made a significant contribution--that render symmetric models increasingly inadequate and which demand refinements. These refinements must reflect dynamical processes within the earth if they are to provide the keys to the earth's past and future evolution.

In addition to the above-mentioned problem in geodesy, the following problem has received considerable attention.

Fluid motion in the liquid core of the earth is widely accepted as the cause of the earth's magnetic field through a dynamo action. For twenty years no general agreement on the driving mechanisms of this fluid motion has been reached, however. Both precessional flow and thermal convection have been proposed and challenged as possible driving mechanisms of the geodynamo. The concept for an experiment described in this work would provide a better understanding of the problem.

The proposed apparatus would consist of a concentric inner sphere and a slightly elliptical outer shell which would be made to rotate and precess. A dielectric fluid would be trapped in the annulus between the two shells and a temperature gradient would be imposed across the annulus. An alternating electric potential between the two shells would create a facsimile gravity field in the annulus. The facsimile gravity is shown to vary as $1/r^5$.

The feasibility of the experiment is discussed both in terms of its power requirements and the differences in flow produced by the strong radial dependence of the facsimile gravity compared to terrestrial gravity. The

working fluid is modelled as a constant viscosity, Boussinesq fluid and the characteristic value problem describing the onset of thermal convection is derived from linearized marginal stability equations. Solution of the characteristic value problem shows that, for an apparatus whose outer shell has major and minor radii of 25 cm and 24 cm, respectively, with a spherical core of 10 cm radius, a 10.5 KV potential is required to create convection at Rayleigh numbers one order of magnitude larger than the critical Rayleigh number of the non-rotating case. The power requirement to generate the electric field is negligibly small in comparison to the heating power requirements, which are estimated to be 1 watt. It is found that the strong radial dependence of the facsimile gravity only affects the magnitude of the critical Rayleigh number, but does not influence the mode of convection. The mode is found to be identical to the mode for constant gravity and for gravity varying as $1/r^2$. At a rotation rate of 20 rpm, it is calculated from the empirical equation of Malkus (1968) that precession rates less than 1 rpm would create unstable precessional flow in the apparatus. The experiment is to be considered feasible in any zero or low gravity laboratory which can provide these power requirements and operating conditions.

The first part of this report describes in detail the proposed zero-gravity geodynamo experiment.

The final sections of the report contain presentations regarding models and proposed experiments for atmospheric flow phenomena.

INTRODUCTION

Zero-gravity laboratories such as the NASA space shuttle offer the unique opportunity to construct physical simulations of three-dimensional and large-scale planetary flows. A currently viable area of planetary fluid dynamics research is the study of fluid motion in rotating, spherical annuli in response to a variety of driving forces. The results of this research are useful in understanding solar rotation phenomena, motion in the earth's oceans and atmosphere, planetary dynamos, and more generally, fluid motion within many planetary interiors. The objective of the experiment described in this work is to study the response of the liquid core of the earth to driving forces created both by thermal buoyancy effects and by the precession of the earth (see Figure 1), although the concept of the experiment may have broader applications. To create a radial, facsimile gravity field in the experiment, a near zero gravity laboratory is required.

The goal of the experiment is to help resolve the apparent dilemma created by Higgins' and Kennedy's 'core paradox' which requires that the radial fluid motion necessary for the geodynamo (Busse, 1975a) must occur in a liquid annulus that is for the most part, thermally stably stratified (Kennedy and Higgins, 1973). On one hand, vigorous radial fluid motion in the earth's liquid core is needed to explain the existence of the earth's magnetic field, while on the other hand, the vigor and possibly the very existence of this fluid motion is limited by the stable stratification of the core.

From the amount of controversy over the driving mechanism of the geodynamo (see Rochester, et al., 1975, and Busse, 1975b), it appears that even the hydrodynamic flow processes occurring within rotating and

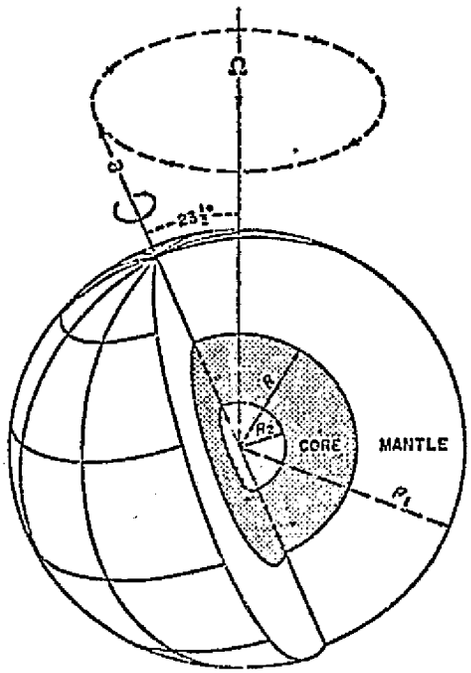

Figure 1. Precesion and Structure of the Earth. Shaded region is liquid core of the Earth, with inner radius R_2 of 1300 km and outer radius R of 3500 km. The axis of rotation of the Earth precesses with a period of 25, 800 years. The angle between the axis of rotation and the axis of precession is 23 1/2 ° (Malkus, 1968).

precessing spheroidal annuli are not well understood. Understanding of the magnetohydrodynamic flow which must actually exist in the geodynamo is probably being delayed by the absence of a strong physical background for evaluating the coupled effects of precessional and thermal buoyancy forces in hydrodynamic flows.

If it is eventually determined that convection can occur in the liquid core, there are still strong reasons to expect the influence of precession to be important in determining the resulting flow patterns. If thermal convection is found to be inadmissable as a driving mechanism of the geodynamo, further study of precessional influences on the flow patterns in the liquid core will be essential (see Young, et al., 1976). The fact that a large fraction of the energy dissipated by the earth-moon system is probably accounted for by precessional flow and that the 'core paradox' appears to impose a restriction on thermal convection in the core strongly supports the need for careful considerations of precessional effects (Young, et al., 1976).

Core convection experiments appear to be a viable topic as a zero-gravity experiment because (1) there seems to be a need to realistically examine the effect of the 'core paradox' on geodynamo models and (2) because core convection experiments require the particular laboratory conditions presently available only in zero or low-gravity environments, the ability to construct radial, spherically symmetric force fields.

Although a physical simulation of a magnetohydrodynamic dynamo is probably impossible to construct (Jacobs, 1974) because electrical and fluid-dynamic processes scale differently, another need for experiments of general hydrodynamic flow in rotating, spheroidal annuli, arises from the fact that current analytical progress and numerical studies of the

problem have dealt only with linear models, with thin shell or other limiting approximations to the fully spherical, thick shell geometry required in a study of the nonlinear flow processes occuring within the earth's core (see, for example, Durney, 1968a, 1968b, and 1970, and Gilman, 1975). Justification of the concept of a zero-gravity geodynamo experiment is ample. The important question is whether or not such an experiment is feasible.

In this work the feasibility of the experiment is examined by determining the conditions for instability in the fluid, both for thermal convection and for precessional flow. Calculation of the conditions needed to produce instability then yields the minimum power supply demand which the experiment imposes on the laboratory. The experiment is considered feasible in any laboratory which can meet this demand.

Four combinations of driving mechanisms are probably relevant to the geodynamo problem: 1) flow driven by simple thermal convection in a rotating spherical annulus; 2) flow driven by precession of a slightly elliptic spherical annulus (see Malkus, 1968); 3) modification of thermal convection by the addition of precession; and 4) modification of precession driven flows by stable thermal stratification. Although the last possibility may be the experiment which addresses the effects of the 'core paradox' most directly, it is the third possibility which makes the largest voltage demand on the laboratory power supply.

Therefore, the calculations presented here are made to estimate the conditions needed to conduct experiment 3. It is assumed that when the conditions necessary for the existence of thermal convection exist simultaneously with the conditions which create precessional instability, both thermal convection and precessional flow will occur.

The effect of the strong radial dependence of the facsimile gravity ($\sim \frac{1}{r^5}$) is also examined by comparing the wave number of the critical Rayleigh number for $g \sim \frac{1}{r^5}$ with that for constant gravity and for $g \sim \frac{1}{r^2}$.

In the absence of a rigorous mathematical treatment of the geodynamo, either by analytical or numerical methods, experiments may be essential for interpreting geodynamo models. The hypothetical experiment described here may provide the most direct means for evaluating the effect of stable thermal stratification and thermal convection on the precessional geodynamo model.

EXPERIMENTAL CONCEPT

Flow in the liquid core of the Earth is characterized by the fact that thermal buoyancy or (in the case of Kennedy and Higgin's 'core paradox') thermal restoring forces do not act in the same direction as the axis of rotation of the core, nor do they act only at right angles to it. Because the direction of thermally-induced body forces varies and because the solid inner core has a radius only 0.4 times the radius of the liquid core surrounding it, fluid flow in the liquid region of the core can be expected to be strongly three-dimensional. The ease with which this potentially complicated flow can be studied by direct observation is a primary impetus for the development of an experiment to model the hydrodynamics of the Earth's liquid core.

The experiment must include the dominant spherical symmetry of the gravitational field, the effects of thermal buoyancy and of inertial forces acting on the fluid. A facsimile, radially symmetric gravitational field can be generated by an electric field acting on a dielectric liquid (see Hart, 1976; Chandra and Smylie, 1972; Gross, 1967; and Smylie, 1966).

The apparatus for a zero gravity, hydrodynamic geodynamo experiment would consist of a concentric inner sphere of radius R_i and a slightly elliptical outer shell of mean radius R_o.[1] The apparatus would rotate and precess, as shown in Figure 2. Trapped in the annulus between the two shells would be a dielectric fluid (e.g., silicone oil). A temperature

---

[1] For practical purposes, R_o can be taken as the major axis radius of the outer shell, so long as the ellipticity of the shell is small.

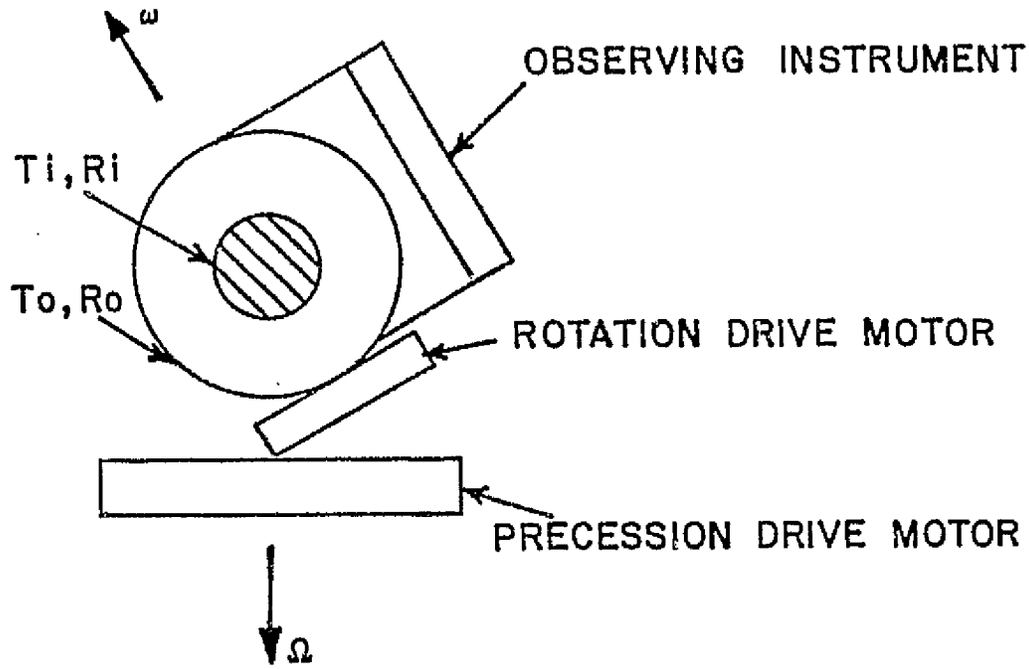

Figure 2. Schematic Diagram of Proposed Apparatus. Proposed laboratory apparatus consists of concentric outer elliptical shell of mean radius R_o, an inner sphere of radius R_i. Temperature of inner annulus surface is T_i, of outer surface T_o. Silicone oil is contained in annulus and the whole apparatus, including ovserving instruments is made to rotate at a rate ω and precess at a rate Ω.

contrast across the annulus gap could be created by circulating a heating or cooling fluid within the inner core and heating or cooling the outside shell, as required. An alternating electric potential ±V is maintained between the outer shell and the core to produce a facsimile gravity field in the model.

A shaft (not shown in the figure) supports the core inside the shell and provides access for heating and cooling the inner core as well as for temperature measuring instrumentation, electrostatic power supply and illumination for flow visualization.

Inertial forces acting on the fluid as a result of the precession of the apparatus would create turbulent motions within the annulus for rates of rotation and precession greater than some critical values. The effect of precessional forces on fluids contained in rotating,precessing and slightly elliptical cavities is to create a cylindrical shear layer extending between ±30° latitude (see Figure 3). Fluid in the central regions of the cavity has a general retrograde (westward) drift while fluid outside of the shear layer shows prograde motion (Malkus, 1968). This cylindrical shear layer will undoubtedly be modified somewhat by the presence of the solid inner core.

Thermal buoyancy forces would be created in the model by the interaction of density gradients and the facsimile gravity field. When unstable thermal gradients would be applied, the chiefly east-west flow generated by precession would interact with the north-south flow caused by thermal convection. In the case of stable thermal stratification, the radial components of the precessional flow would be suppressed by thermal buoyancy forces.

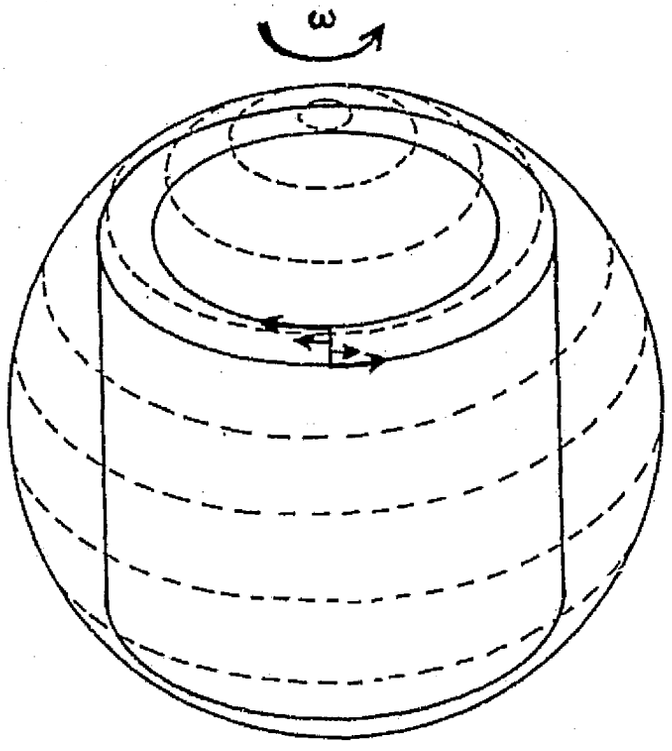

Figure 3. Precessional Shear Layer. The cylindrical shear layer observed by Malkus (1968) within a fluid contained in a rotating and precessing elliptical cavity is shown in exaggerated form in this figure. With increasing rates of rotation and precession the shear layer becomes unstable, developing wave-like motions and finally turbulence.

Because the electric field generating the facsimile gravity field cannot be made strong enough to overcome the external gravity in the terrestrial laboratories without creating electrical breakdown of the dielectric fluid (Hart, 1976), the experiment must be performed in zero or low gravity laboratories.

To permit visualization of flow fields by tracer motions or dye streaks, the upper hemisphere of the outer shell would be constructed of glass or plexiglass with a thin, transparent coating of a metallic oxide to make it electrically conducting. The inner core could also be constructed of coated glass or plexiglass, permitting the use of shadow graph or Schlieren flow visualization techniques (see Hart, 1976).

In contrast to the flow visualization needs for convection experiments in rotating, spherical annuli, the needs for visualizations and data obtained from the experiments described here include making records of east-west fluid motion as well as north-south fluid motion. The motion on latitudinal planes is important, as it reflects the contribution of precessional flow to the resulting fluid motion, while motion on longtitudinal planes indicates the contribution of thermal convection.

Stable thermal stratification is created by heating the outer shell while cooling the inner core. Unstable thermal stratification is created by heating the inner core and cooling the outer boundary as in Chandra and Smylie(1972).Precessional instability is created by increasing the rate of rotation or rate of precession of the apparatus.

The electric thermal buoyancy forces are created in the experiment by the interaction of the temperature-dependent dielectric constant and the imposed electric field. When the dielectric constant decreases with increasing temperature (see Figure 4), warm liquid seeks regions of less

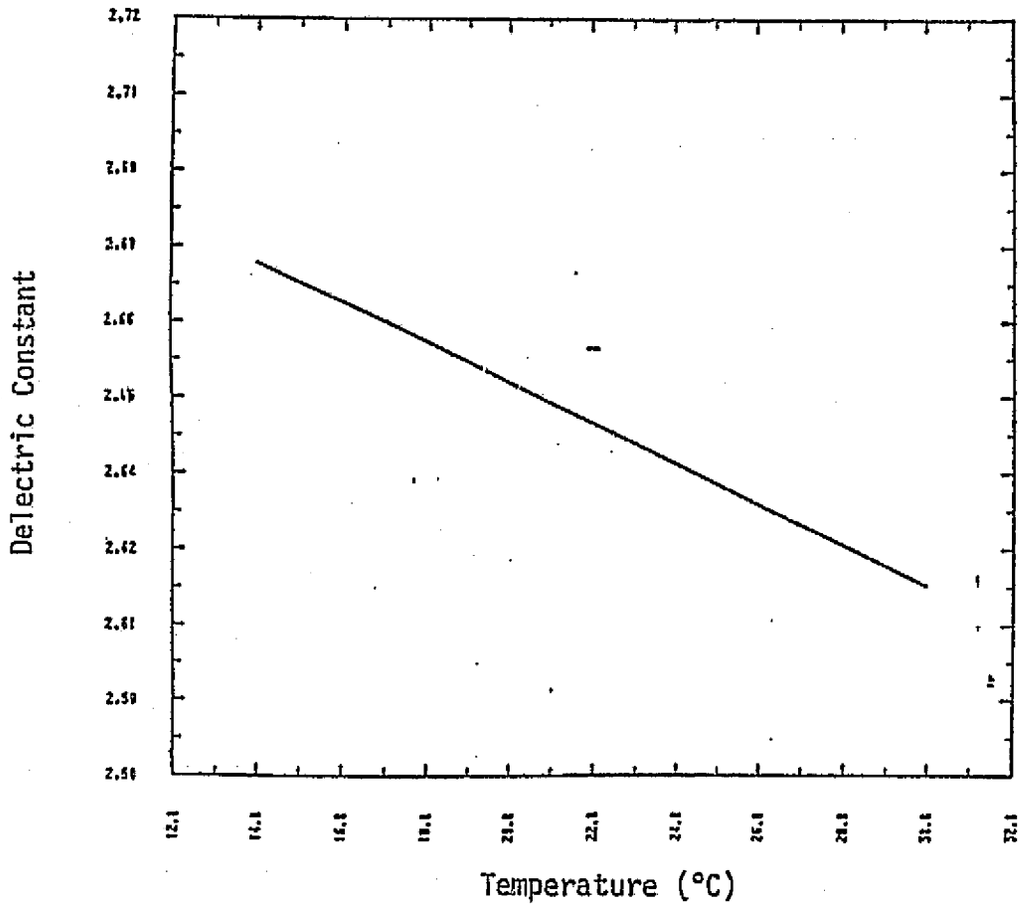

Figure 4. Dielectric Constant vs. Temperature. Temperature dependence of dielectric constant in a typical silicone oil (after Chandra and Smylie, 1972).

intense electric field while cold liquid seeks regions of more intense electric field (Chandra and Smylie, 1972).

Another flow may be generated in the fluid due to the migration of free charges. This 'streaming flow' limits the accuracy of the simulation as it introduces a transport mechanism which is not found in terrestrial thermal convection. An alternating electric field must be applied to prevent the occurrence of the 'streaming flow.'

At this point the concept of a zero-gravity, hydrodynamic geodynamo experiment has been defined. ıe physical design of the apparatus must wait until the needed boundary conditions have been determined, however. In the next section the boundary conditions for thermal convection are estimated; the boundary conditions for precessional flow are estimated in a later section.

ONSET OF THERMAL CONVECTION

The onset of convection in the annulus is determined by the critical Rayleigh number, which is defined as the product of the Prandtl and Grashof numbers. The Grashof number represents the ratio of buoyant to viscous forces in the fluid. The Prandtl number relates temperature and velocity distributions in the fluid.

An eigenvalue problem is formulated from the governing equations in which the characteristic value is the Rayleigh number and the mode represents the temperature distribution. The problem is formulated by substituting simple forms of perturbations of the state variables into the momentum, heat and continuity equations, yielding the perturbation equations. An exponential time-dependence of these perturbations is then assumed, and the marginal stability equations are derived from the perturbation equations. The eigenvalue problem is formulated directly from the marginal stability equations. (See Chandrasekhar, 1961.)

In this work, derivation of the perturbation equations is taken directly from the work of Durney (1968a). The derivation is only briefly described here to provide the background needed to understand the marginal stability equations.

In calculating critical Rayleigh numbers by this method, it has been assumed that the apparatus consists of two non-rotating, concentric spheres. The first assumption is made in order to decouple the different modes of convection, simplifying the problem by eliminating terms in the governing equations (see Durney, 1968b). As a consequence, the calculated Rayleigh number represents a minimum Rayleigh number of interest in the experiment. Fluid viscosity is assumed to be constant.

The second assumption is reasonable since the inner boundary is spherical and the outer boundary is nearly spherical.

Before deriving the eigenvalue problem, we must determine the form of the electrical "gravity" field. The next section is devoted to this.

A. Electric Body Forces

The electric body force per unit volume exerted on the fluid is (Chandra and Smylie, 1972)

$$\vec{f} = 1/2\ \rho' \nabla \left[E_o^2 \left(\frac{\partial \varepsilon}{\partial \rho}\right)_{T,o}\right] - 1/2\ E_o^2 \left(\frac{\partial \varepsilon}{\partial T}\right)_{\rho,o} \nabla T' \qquad (1)$$

where primes indicate flow-induced quantities and subscripted zeroes indicate stationary values. E_o is the electric field strength, ε is the dielectric permittivity, T is the temperature.

The permittivity of a material is calculated by multiplying the material's dielectric constant and the universal constant ε_o, the permittivity of free space. In mks units ε_o has the value 8.854×10^{-12} farads per meter.

The dielectric constant κ of a material is defined as the ratio of the electric field strength in a vacuum to that in the material, for the same distribution of charge (Smyth, 1955). Another definition makes use of the ratio of the capacitance of a flat plate condenser with a vacuum between the plates (C_o), and the same condenser with the material between the plates. The dimensionless dielectric constant is defined as

$$\kappa = \frac{C}{C_o}$$

A typical dielectric constant for silicone oils used in convection experiments is $\kappa = 2.65$ (see, for example, Chandra and Smylie, 1972).

The departure of density from its stationary value is

$$\rho' = -\alpha\rho_o T' \qquad (2)$$

and the fluid state is given by

$$T = T' + T_o$$

$$p = p' + p_o$$

$$\rho = \rho' + \rho_o$$

where p is the pressure and α is the volume coefficient of expansion. Again, subscripted zeroes indicate stationary conditions (no fluid motion, purely hydrostatic pressure field, temperature distribution that of pure conduction), and primes denote flow-induced quantities.

Substituting (2) into (1) and dividing by ρ_o gives the electrical body force per unit mass

$$\vec{F} = -1/2\ \alpha T'\ \nabla\left[E_o^2\left(\frac{\partial\varepsilon}{\partial\rho}\right)_{T,o}\right] - 1/2\ 1/\rho_o\ E_o^2\left(\frac{\partial\varepsilon}{\partial T}\right)_{\rho,o}\ \nabla T'$$

Assuming density and permittivity changes are small, $\left(\frac{\partial\varepsilon}{\partial\rho}\right)_{T,o}$ will be independent of the spatial coordinates and the body force per unit mass becomes

$$\vec{F} = -1/2\alpha\left(\frac{\partial\varepsilon}{\partial\rho}\right)_{T,o}\nabla E_o^2\ T' - 1/2\ 1/\rho_o\ E_o^2\left(\frac{\partial\varepsilon}{\partial T}\right)_{\rho,o}\ \nabla T'$$

It is the curl of the body force which we will use in the equation of motion, or

$$\nabla \times \vec{F} = -1/2\,\alpha \left(\frac{\partial \varepsilon}{\partial \rho}\right)_{T,o} \nabla T' \times \nabla E_o^2 \; -1/2\; 1/\rho_o \left(\frac{\partial \varepsilon}{\partial T}\right)_{\rho,o} \nabla E_o^2 \times \nabla T'$$

Equivalently, since the two vector components of $\nabla \times F$ are co-linear

$$\nabla \times \vec{F} = 1/2 \;\; \left[1/\rho_o \left(\frac{\partial \varepsilon}{\partial T}\right)_{\rho,o} - \alpha \left(\frac{\partial \varepsilon}{\partial \rho}\right)_{T,o}\right] \nabla T' \times \nabla E_o^2$$

The permittivity coefficients must also satisfy the relation

$$1/\rho_o \left(\frac{\partial \varepsilon}{\partial T}\right)_{\rho,o} - \alpha \left(\frac{\partial \varepsilon}{\partial \rho}\right)_{T,o} = 1/\rho_o \left(\frac{\partial \varepsilon}{\partial T}\right)_{p,o}$$

from thermodynamics (Chandra and Smylie, 1972). Thus the curl of the body force may be written

$$\nabla \times \vec{F} = \frac{1}{2\,\rho_o} \left(\frac{\partial \varepsilon}{\partial T}\right)_{p,o} \nabla T' \times \nabla E_o^2 \qquad (3)$$

By analogy to the terrestrial thermal buoyancy force

$$\vec{F} = \alpha T' \nabla \phi$$

where $g = \nabla \phi$ and ϕ is the geopotential, it can be shown that the electric, facsimile gravity in (3) may be written

$$g_e = \frac{1}{2\,\alpha \rho_o} \left(\frac{\partial \varepsilon}{\partial T}\right)_{p,o} \nabla E_o^2 \qquad (4)$$

The electric field E in a spherical capacitor with inner radius R_i, outer radius R_o, and annulus gap a is (Moore, 1973)

$$E = V \left\{ \frac{R_i R_o}{a} \right\} \quad \frac{1}{r^2}$$

where V is the voltage across the capacitor. Inserting this in (4) we obtain the useful expression for the electric facsimile gravity

$$g_e(r) = \frac{2}{\alpha \rho_o} \left(\frac{\partial \varepsilon}{\partial T}\right)_{p,o} V^2 \left\{\frac{R_i R_o}{a}\right\}^2 \frac{1}{r^5} \qquad (5)$$

The radial dependence of g_e remains a major difference between the facsimile gravity field and the gravity field which actually exists within the interior of the earth, although this difference may be most noticeable only at the onset of thermal convection (Gilman, 1976). Other kinds of radial dependence can be produced in facsimile gravity fields by the use of other geometries for generating the electric field, as shown in Table I.

Table I

Geometry	Electric Field	Facsimile Gravity
plane	constant	none
cylindrical	$1/r$	$1/r^3$
spherical	$1/r^2$	$1/r^5$

Only with spherical geometry does the facsimile gravity field posess the spherical symmetry found in the earth's gravitational field, however.

B. Formulation of the Eigenvalue Problem

Consider a stationary spherical annulus of thickness a filled with a fluid of density ρ_o. The acceleration of gravity within the annulus is

$$g_e(r) = \frac{2}{\alpha \rho_o} \left(\frac{\partial \varepsilon}{\partial T}\right)_{p,o} V^2 \left\{\frac{R_o R_i}{a}\right\}^2 \frac{1}{r^5}$$

The outer radius of the annulus is R_o, its inner radius $\eta R_o = R_i$. The velocity field $\vec{u}$, temperature T, radial coordinate r and time t are scaled by the following definitions:

$$\vec{u} = \frac{K}{R_o} \vec{u}'; \quad T = |T_o| \; T'; \quad r = R_o r'$$
$$t = \frac{R_o^2}{K} t'; \quad g(r) = g(R_o) \; g'(r') \tag{6}$$

K is the thermal diffusivity and T_o is the negative temperature of the outer boundary of the annulus. (The temperature at the inner boundary is assumed to be zero.) All primed quantities are dimensionless.

Dropping the primes in (6), the nondimensional momentum, continuity and heat equations of the problem can be written as (Durney, 1968a)[2]

$$\frac{1}{P_r} \frac{\partial}{\partial t} \nabla \times \vec{u} - \nabla \times \nabla^2 \vec{u} = -\frac{1}{P_r} \nabla \times (\vec{u} \cdot \nabla) \vec{u} + R_1 \nabla \times g(r) \vec{r} \, T$$

$$\nabla \cdot \vec{u} = 0$$

and

$$\left(\frac{\partial}{\partial t} - \nabla^2\right) T = -\nabla \cdot (\vec{u} \, T)$$

P_r is the Prandtl number

---

[2]It should be noted that this is the curl of the momentum equation, as the pressure term ∇p is absent.

$$P_r = \frac{\nu}{K}$$

and R_1 is the Rayleigh number based on the radius of the outer annulus boundary,

$$R_1 = \frac{\alpha |T_o| g(R_o) R_o^3}{K \nu}$$

Another common form of the Rayleigh number is based on the annulus depth a

$$R_a = \frac{\alpha |T_o| g(R_o) a^3}{K \nu}$$

and is related to the outer radius Rayleigh number R_1 by (Durney, 1968a)

$$R_a = R_1 \left[\frac{a}{R_o} \right]^3$$

Equivalently,

$$R_a = R_1 (1-\eta)^3$$

Substituting equation (5) into the definition of R_1 we obtain

$$R_1 = \frac{\Delta T V^2 \left(\frac{\partial \varepsilon}{\partial T} \right)_{p,o} \frac{\dot{2}}{\rho_o} \frac{\eta^2}{(1-\eta)^2}}{K \nu}$$

the useful form of the Rayleigh number.

Durney (1968a) has derived the perturbation equations by assuming a temperature distribution of the form

$$T = \frac{1}{1-\eta} \left[\frac{\eta}{r} - 1 \right] + \psi(r,t) + \theta(\hat{r}, t)$$

The first term represents the temperature field of pure conduction with boundary conditions T = 0 at the inner boundary and T = -1 at the outer boundary. It is a solution of Laplace's equation $\nabla^2 T = 0$ in spherical co-ordinates. ψ (r,t) represents the mean distortion of the temperature field by convection and is a function of the radial coordinate and time. θ ($\hat{r}$, t) is expanded in spherical harmonics by writing

$$\theta(\hat{r},t) = \sum_{L,m} \theta_{L,m}(r,t)\, y_L^m(\theta,\phi)$$

where y_L^m is the spherical harmonic and is a known function of θ , ϕ , and wave numbers L and m. Thus the temperature field is completely determined by specifying only two functions, $\theta_{L,m}(r,t)$ and $\psi(r,t)$, both of which are functions of radius and time only.

Similarly a specific form for the velocity is assumed using the poloidal vector $\vec{P}_{L,m}$

$$\vec{u} = \sum_{L,m} \vec{P}_{L,m}(p_{L,m})$$

which has the following components in spherical co-ordinates

$$P_{L,m}^{(r)} = \frac{(L+1)\,L}{r^2} P_{L,m}(r,t)\, y_L^m(\theta,\phi)$$

$$P_{L,m}^{(\theta)} = \frac{1}{r} \frac{\partial P_{L,m}(r,t)}{r} \frac{y_L^m(\theta,\phi)}{\partial\phi}$$

and

$$P_{L,m}^{(\phi)} = \frac{1}{r \sin\theta} \frac{\partial P_{L,m}(r,t)}{\partial r} \frac{y_L^m(\theta,\phi)}{\partial\phi}$$

Thus the velocity field is completely described by determining a function $P_{L,m}(r,t)$ which is a function of radius and time only.

The convection problem is solved by finding the required functions $P_{L,m}(r,t)$, $\theta_{L,m}(r,t)$ and $\psi(r,t)$. From the momentum, continuity, and heat equations, Durney (1968a) derived three equations governing these variables, the perturbation equations

$$D_L^2 P_{L,m} = R_1 g(r) \theta_{L,m} \qquad 8(a)$$

$$\frac{\partial \psi}{\partial t} - D_L \psi - \frac{(L+1)L}{r^2} \psi =$$

$$- \frac{1}{4\pi r^2} \sum_{L,m} (L+1)L \frac{\partial}{\partial r} (r P_{L,m} \vartheta_{L,m}) \qquad 8(b)$$

and

$$\frac{\partial \theta_{L,m}}{\partial t} - D_L \theta_{L,m} = \frac{(L+1)L}{r} P_{L,m} \left[\frac{\eta}{(1-\eta) r^2} - \frac{\partial \psi}{\partial r} \right]$$

$$8(c)$$

where D_L is the differential operator

$$D_L = \frac{d^2}{dr^2} + \frac{2}{r} \frac{d}{dr} - \frac{(L+1)L}{r^2}$$

and, for his own convenience, Durney has redefined $P_{L,m}$ as

$$P_{L,m} = \frac{P_{L,m}(r,t)}{r}$$

The boundary conditions on the temperature variables are $\psi = \theta_{L,m} = 0$ at $r = \eta, 1$. Either rigid or free boundary conditions are used for the velocity, as required.

Since we are interested in those small perturbations which start convection, $\theta_{L,m}$, ψ , and $p_{L,m}$ may be assumed to be small. By ignoring products of the perturbations with themselves and their derivatives the linearized perturbation equations may be obtained

$$D_L^2 \; P_{L,m} = R_1 \; g(r) \; \theta_{L,m} \qquad 9(a)$$

$$\frac{\partial \psi}{\partial t} - D_L \; \psi - \frac{(L+1)L}{r^2} \; \psi = 0 \qquad 9(b)$$

and

$$\frac{\partial \theta_{L,m}}{\partial t} - D_L \; \theta_{L,m} = \frac{(L+1)L}{r^3} \; P_{L,m} \; \frac{\eta}{(1-\eta)} \qquad 9(c)$$

Note that different values of wave number L are decoupled and that the equations are m independent. Since the term containing a sum over m terms in 8(b) has vanished in the linearization process, however, the governing equations themselves are independent of m and the subscript will be dropped.

The marginal stability equations are obtained from the linearized perturbation equations by assuming an exponential time dependence in the state variables. The perturbed temperature distribution will be described, for example, by the product of a function of time and a function A describing the amplitude of the perturbation in terms of the spatial coordinates:

$$T(\hat{r}, t) = e^{pt} A(\hat{r})$$

The conditions for stability are clearly

$p > 0$: unstable

$p = 0$: marginally stable

$p < 0$: stable

Thus the marginal stability equations are obtained by setting the exponent p to zero in the perturbation equations.

The three functions used to describe the temperature and velocity fields are rewritten with the exponential time dependence

$$\theta_L(r,t) = e^{pt}\ \theta_L(r)$$

$$\psi(r,t) = e^{pt}\ \psi(r)$$

and

$$p_L(r,t) = e^{pt}\ p_L(r)$$

Substituting these definitions into the linearized perturbation equations under marginal stability conditions (p=0), all time derivatives disappear and the time-dependent terms become unity. The result is the marginal stability equations

$$D_L^2 P_L = R_1\, g(r)\ \theta_L \qquad 10(a)$$

$$D_L \psi + \frac{(L+1)L}{r^2}\ \psi = 0 \qquad 10(b)$$

$$D_L \theta_L = \frac{(L+1)L}{r^3}\ P_L\ \frac{\eta}{(1-\eta)} \qquad 10(c)$$

Equation (10c) can be written as

$$P_L = \frac{r^3(n-1)}{\eta L_1} \; D_L \cdot \theta_L$$

where $L_1 \equiv (L+1)L$. Inserting this expression into equation (10a) yields the eigenvalue problem in terms of the temperature variable θ_L,

$$D_L^2 \left[\frac{r^3(n-1)}{\eta L_1} \; D_L \; \theta_L \right] = R_1 \; g(r) \; \theta_L$$

in which the Rayleigh number R_1 is the characteristic value and the temperature distribution θ_L is the corresponding mode. By operating the differential operator D_L upon itself the differential operator D_L^2 may be obtained

$$D_L^2 = \frac{d^4}{dr^4} + \frac{4}{r} \frac{d^3}{dr^3} - \frac{2L_1}{r^2} \frac{d^2}{dr^2} + \frac{L_1^2 - 2L_1}{r^4}$$

We note that the definition of the non-dimensional gravity term $g'(r)$ when applied to the electrical gravity yields (see equation (6))

$$g'(r) = \frac{g(r)}{g(R_o)} = \frac{1}{r^5}$$

Using the definitions of D_L and D_L^2 the eigenvalue problem may be written as

$$\frac{d^6 \theta_L}{dr^6} + \frac{18}{r} \frac{d^5 \theta_L}{dr^5} + \frac{96-3L_1}{r^2} \frac{d^4 \theta_L}{dr^4} \qquad \text{(continued)}$$

$$+\frac{168-24L_1}{r^3}\quad\frac{d^3\theta L_1}{dr^3}+\frac{3L_1^2-42L_1+72}{r^4}\quad\frac{d^2\theta_L}{dr^2}$$

$$+\frac{6L_1^2-12L_1}{r^3}\quad\frac{d\theta_L}{dr}-\frac{L_1^3-2L_1^2}{r^6}\quad\theta_L=$$

$$\frac{\eta L_1}{\eta-1}\quad\frac{R_1}{r^8}\quad\theta_L \qquad (11)$$

This is the basic equation of the eigenvalue problem. With the six boundary conditions derived in the next section, formulation of the problem describing the onset of convection is complete.

No-slip (rigid) boundary conditions on the velocity and constant temperature at inner and outer annulus boundaries are used. The temperature boundary condition is

$$\theta_L(r) = 0 \text{ at } r = \eta, 1 \qquad (12a)$$

and

$$\psi(r) = 0 \quad \text{at } r = \eta, 1$$

The no-slip condition requires that all components of velocity vanish at the boundaries, or

$$P_L(r) = P_L(\theta) = P_L(\phi) = 0 \text{ at } r = \eta, 1.$$

By the definitions of the components of the velocity, it is apparent that only two conditions are needed to make $\vec{u}$ vanish at the boundaries. These are

$$p_L(r) = 0 \text{ at } r = \eta, 1$$

and

$$\frac{\partial P_L(r)}{dr} = 0 \quad \text{at } r = \eta, 1$$

Using the former in equation (9c) we obtain $D_L\ \theta_L = 0$ at $r = \eta, 1$. (12b)

Substituting the definition $P_L = \frac{p_L}{r}$ into (10c)

$$D_L\ \theta_L = \frac{L_1}{r^4} \qquad \frac{\eta}{\eta - 1} \qquad p_L$$

The requirement $\frac{dp_L(r)}{dr} = 0$ can be restated using this expression as

$$\frac{d}{dr}\ [r^4\ D_L\ \theta_L] = 0 \tag{12c}$$

Upon substituting the definitions of the differential operators into equations (12) we obtain the boundary conditions in their useful form:

$$\theta_L = 0 \quad \text{at } r = \eta, 1 \tag{13a}$$

$$\frac{d^2\ \theta_L}{dr^2} + \frac{2}{r}\ \frac{d\theta_L}{dr} - \frac{L_1}{r^2}\ \theta_L = 0 \text{ at } r = \eta, 1 \tag{13b}$$

and

$$\frac{d^3\theta_L}{dr^3} + \frac{6}{r}\ \frac{d^2\ \theta_L}{dr^2} + \frac{6 - L_1}{r^2}\ \frac{d\ \theta_L}{dr} - \frac{2L_1}{r^3}\ \theta_L = 0 \text{ at } r = \eta, 1 \tag{13c}$$

Thus equation (11) is the governing equation for the eigenvalue problem and equations (13) are the six boundary conditions needed to solve it.

C. Numerical Solution

The eigenvalue problem (11) and associated boundary conditions (13) were solved by using the finite-difference method and the edition 5 International Mathematics and Statistics Library (IMSL) eigenvalue subroutine EIGZF (see Appendix I). The domain $\eta \leq r \leq 1$ was modelled with 37 nodal points. It should be noted that the only solution to (10b) which satisfies the boundary conditions is $\psi(r) = 0$. The temperature distribution within the annulus is therefore given by

$$T = \frac{1}{1-\eta}\left[\frac{\eta}{r} - 1\right] + \theta(\hat{r}, t)$$

Because (11) is homogeneous, any multiple of a given solution $\theta_L(r)$ is also a solution.

Solutions were obtained for $\eta = 0.4$, rigid boundaries and $g \sim \frac{1}{r^5}$ to estimate critical Rayleigh numbers for the experimental apparatus. To evaluate the influence of the strong radial dependence of the radial gravity on the mode of convection, solutions were obtained with free boundaries (see Appendix III) with $\eta = 0.8$, $g \sim 1/r^5$. These results were compared with the results of Durney (1968a) and Gilman (1975) which were obtained with constant gravity and with $g \sim 1/r^2$, respectively. Verification of equation (11) as a model of thermal convection in the annulus was obtained by (1) repeating the result of both Durney (1968a) and Gilman (1975) and (2) demonstrating that the model predicts higher

critical Rayleigh numbers for rigid boundaries than for free boundaries. The results are summarized in Table II.

Sol'n.	Gravity	n	Boundaries	L	R_a
1	const.	0.8	free	9	740
2	$1/r^2$	0.8	free	9	596
3	$1/r^5$	0.8	free	9	426
4	$1/r^5$	0.4	free	3	142
5	$1/r^5$	0.4	rigid	3	295

Table II

Summary of Numerical Results

Solutions (1) and (2) reproduce within 5% the results of Durney (1968a) and Gilman (1975), respectively, indicating that the linear model of convection represented by equation (11) with the free surface boundary conditions is in general agreement with nonlinear models of convection. Solutions (4) and (5) demonstrate that the linear model with rigid boundary conditions is also consistens with physical intuition (Durney, 1976), because the model predicts higher critical Rayleigh numbers for rigid boundaries than for free boundaries. Higher Rayleigh numbers for rigid boundaries are to be expected, since in that case thermal buoyancy forces must overcome viscous forces both in the bulk of the fluid and at the fluid boundaries for convection to occur. With free boundaries buoyancy forces must overcome viscous forces only in the bulk of the fluid to initiate convection.

Comparison of solutions (1), (2), and (3) shows that the effect of the strong radial dependence of the facsimile gravity only alters the value of the critical Rayleigh number. For g $1/r^5$, the critical Rayleigh number occurs at a wave number L = 9 (see Figure 5), as did the critical Rayleigh numbers calculated by both Durney (1968a) and Gilman (1975) for constant gravity and g $1/r^2$, respectively. The spectrum of Rayleigh numbers over a wide range of wave numbers is shown in Figure 5. Figure 6 shows the critical mode and temperature distribution in the rigid boundary case.

Since the effect of rotation on thermal convection in spherical annuli is to suppress fluid motion and therefore increase the critical Rayleigh number (Gilman, 1975), the results calculated here represent the bottom of the range of important Rayleigh numbers for the experiment. It will probably be desirable to conduct experiments over the range of Rayleigh numbers from the minimum to at least an order of magnitude or more above the minimum.

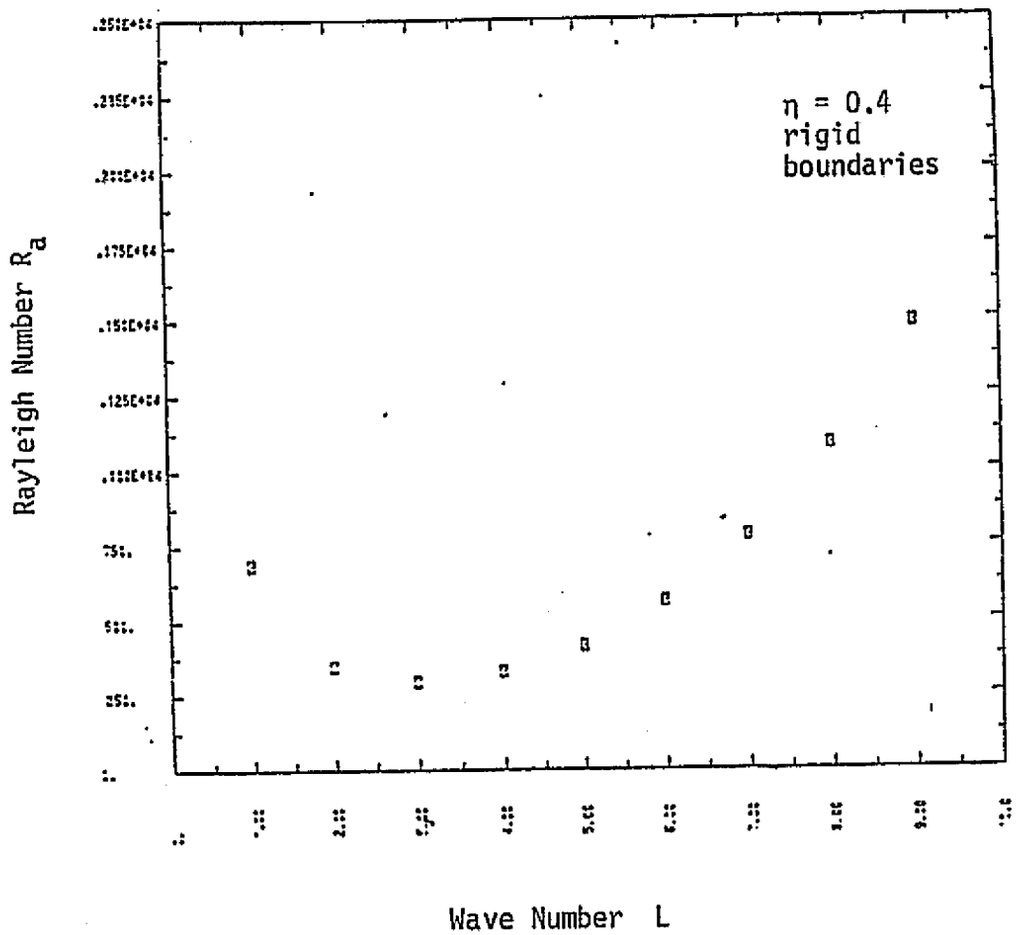

Figure 5a. Rayleigh Number vs. Wave Number L for η = 0.4 and rigid boundary conditions. Minimum Rayleigh number of 295 occurs at a wave number of 3.

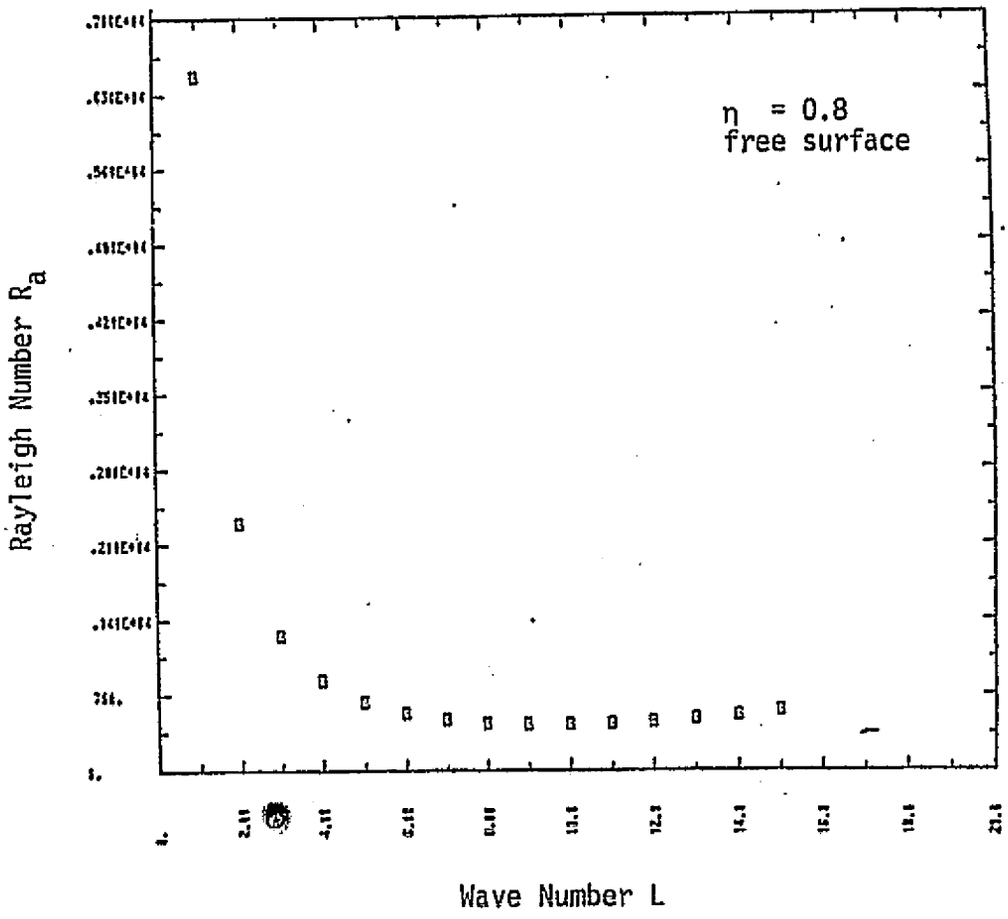

Figure 5b. Rayleigh number vs. wave number L for η = 0.8 and free surface boundary conditions. Minimum Rayleigh number of 426 occurs at a wave number of L = 9 and L = 10.

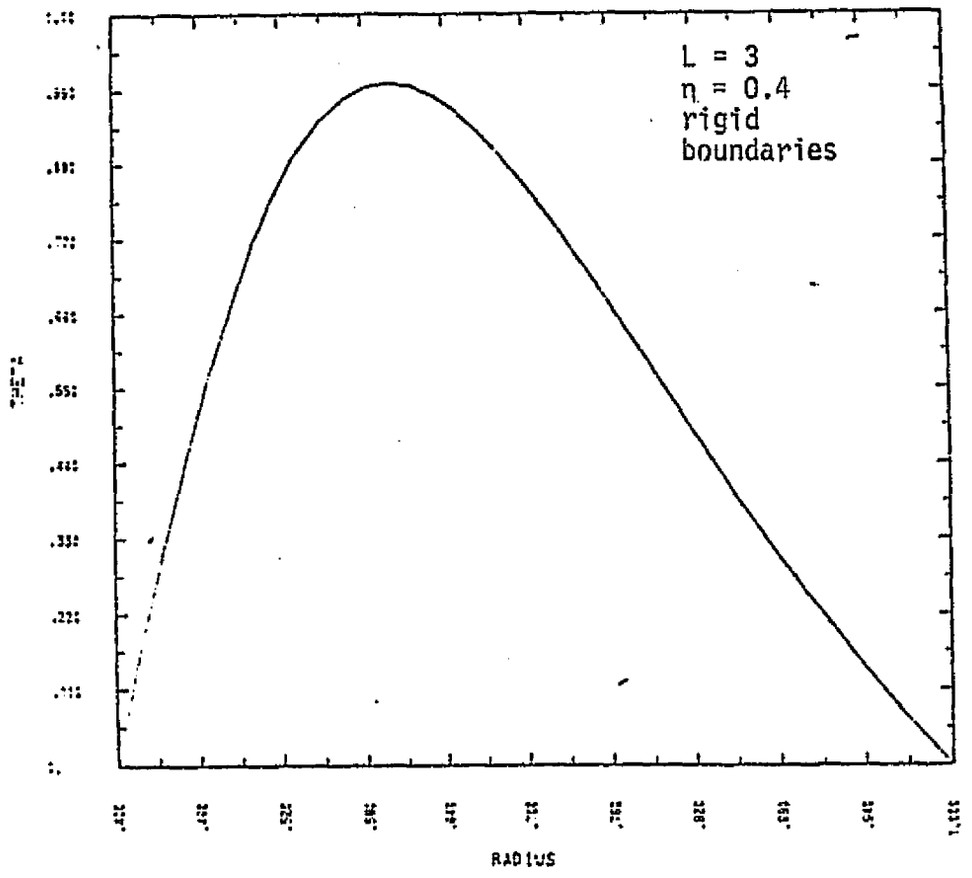

Figure 6a, Critical Mode. Plot shows θ_L, L = 3, from inner annulus boundary to outer annulus boundary. θ_L is arbitrarily normalized so that its largest element is unity. For a free surface boundary solution to the same problem, see Appendix III.

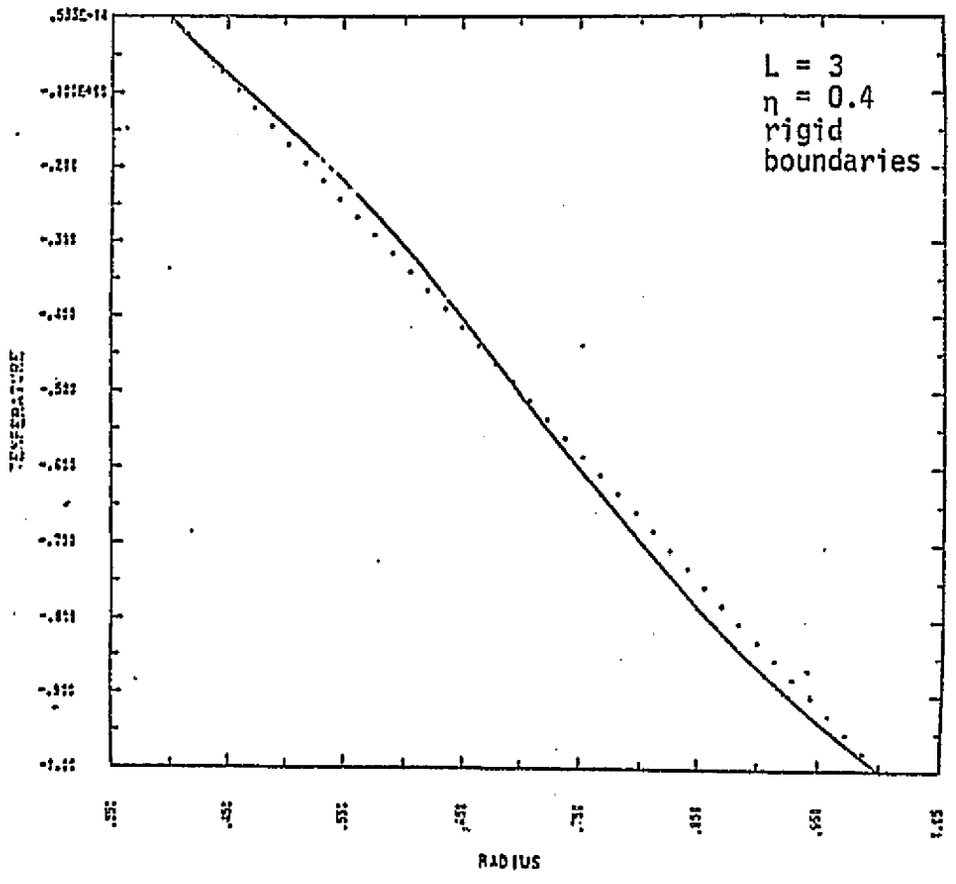

Figure 6b. Temperature Profile. Dotted line shows profile of pure conduction, solid line shows sum of conduction profile and θ_L, L = 3. θ_L has been arbitrarily normalized so its length is unity. For a free surface solution of the same problem, see Appendix III.

Precessional Flow

The equation of motion of a viscous fluid inside the spheroidal cavity of a precessing rigid body which is rotating about its axis with a constant angular velocity w_s is

$$2\vec{\Omega} \times \vec{q} + \vec{q} \cdot \nabla\vec{q} = -\nabla p + E \nabla^2 \vec{q}$$

where $\vec{\Omega}$ is the angular velocity of the rotating frame of reference, p is the pressure and q is the fluid velocity (Busse, 1968).

This equation illustrates the fact that equality of the Eckman numbers

$$E = \frac{\nu}{\omega R^2}$$

for two precessional flows will establish dynamic similarity between, for example, the liquid core of the earth and a laboratory experiment. Some physical properties of and vertical velocity in the earth's liquid core are shown in Table III. These figures yield an Eckman number for the core of

$$E = 6.72 \times 10^{-16}$$

based on the radius of the earth's outer core, 3500 km. Figure 7 shows that in a feasibly-sized apparatus rotated at speeds below 5000 rpm, Eckman numbers in a laboratory experiment will be much larger than in the earth's core. Although it appears impossible to establish dynamic similarity between the experiment and the core, previous experiments with fluid motion in rotating and precessing cavities indicate that instabilities and turbulence can be made to occur for $E > 10^{-5}$ (Malkus, 1968). Thus fluid motion of interest can be created in a physical simulation of the earth's liquid core.

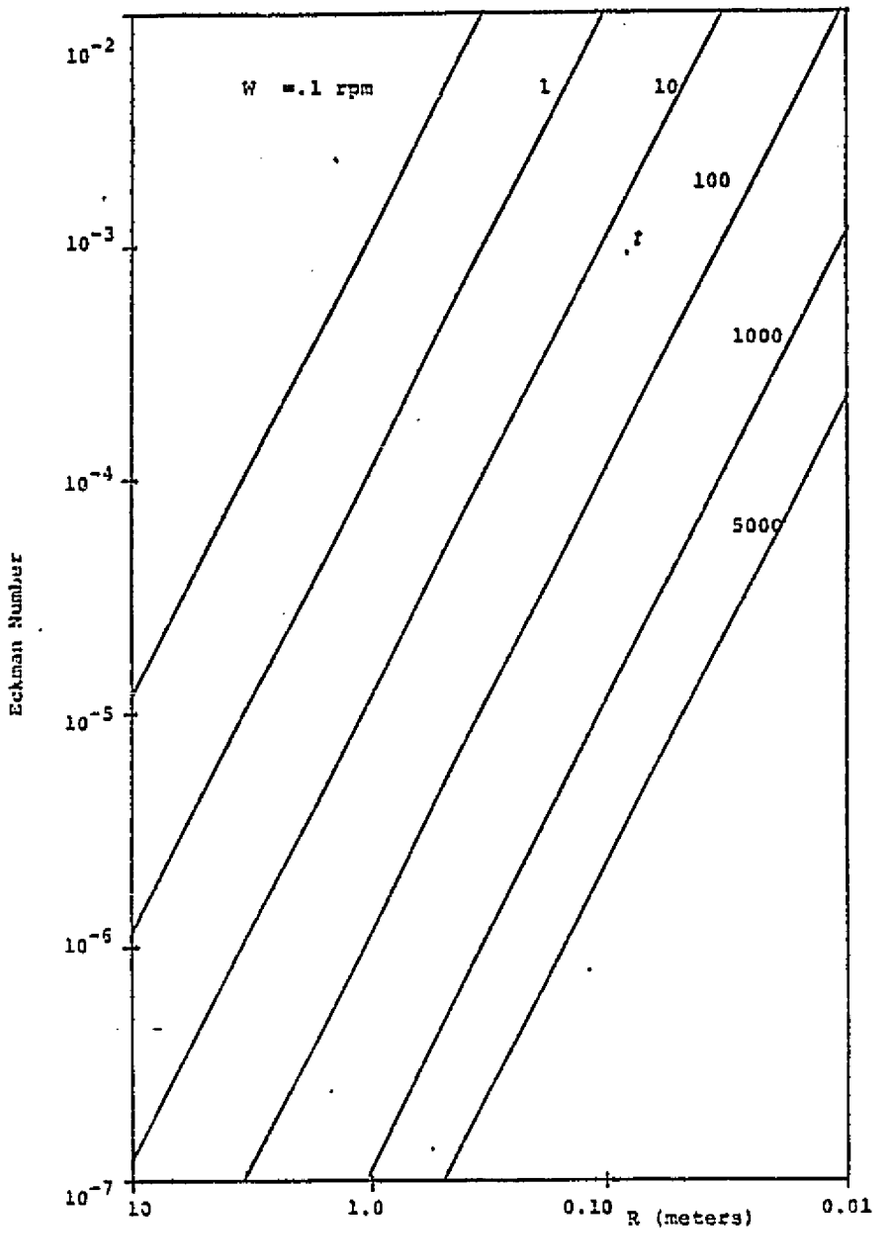

Figure 7. Eckman numbers in the laboratory experiment. R is the mean radius of the outer shell. (ν = 12 CS, after Chandra and Smylie, 1972).

Property	Value	Reference
Specific Heat	7.12×10^2 $Jkg^{-1}°K^{-1}$	Frazer (1973)
Coefficient of Thermal Expansion	$4.5 \times 10^{-6}°K^{-1}$	Frazer (1973)
Thermal Conductivity	60 $W\ m^{-1}°K^{-1}$	Frazer (1973)
Radial Fluid Velocity	3×10^{-4} $m\ s^{-1}$	Frazer (1973)
Kinematic Viscosity	0.6 centistokes	Gans (1972)
Mass Density	13 $gm\ cm^{-3}$	Gans (1972)

Table 3. Physical Properties of and vertical velocity in the Earth's liquid core

Onset of instability in a fluid contained in a rotating and precessing spheroid can be determined from an empirical equation relating the ratio A of the maximum toroidal velocity in the fluid to the speed of the periphery of the container.

Instability occurs when

$$A > (5.0 \pm 0.3)\, E^{1/2} \qquad (14)$$

where E is the Eckman number,

$$E = \frac{\nu}{\omega R_m^2}$$

R_m is the mean radius of the spheroid, and ω is the rotation rate about the sphere's minor axis (Malkus, 1968). A is determined from the rotational velocity of the container (w) and the rate of precession (Ω)

$$A = \frac{|\vec{\omega} \times \vec{\Omega}|^2}{|\vec{\omega}|^2 e^2} f(E) \qquad (15)$$

where e is the ellipticity of the spheroid,

$$e = \frac{I_p - I_E}{I_p}$$

(see Malkus, 1968). I_p is the moment of inertia of the spheroid about its "polar" (minor) axis and I_E is its moment of inertia about the "equatorial" (major axis).

In (15) f(E) is defined by

$f(E) = 0.4$, $E > 10^{-5}$

$f(E) \simeq E^{-1/6}$, $E < 10^{-7}$

Combining the definition of the Eckman number and expression (15) for A with equation (14), we find the required rate of precession for instability to be

$$\Omega > \frac{e}{\sin\theta} \quad \frac{5}{f(E)} \quad \left\{\frac{\gamma}{\omega R_m^2}\right\}^{1/4} \tag{16}$$

For an elliptical body with a major axis R_{maj} and minor axis R_{min} the moment of inertia about the pole (minor axis) is

$$I_p = \frac{M}{5}(2\,R_{maj}^2)$$

and the moment of inertia about the equator (major axis) is

$$I_E = \frac{m}{5}(R_{maj}^2 + R_{min}^2)$$

so the dynamic ellipticity of the body is

$$e = \frac{R_{maj}^2 - R_{min}^2}{2R_{maj}^2}$$

Malkus (1968) found that instability in the precessional flow first manifests itself as wave motions with the cylindrical shear layer depicted in Figure 3. The waves move retrograde (west) relative to the rotation of the spheroid. For a given rate of precession, instabilities are intensified by decreasing the Eckman number of the flow.

EXPERIMENTAL APPARATUS

The critical Rayleigh number for convection in the experimental apparatus was calculated to be $R_a = 295$. Using the definition of the Rayleigh number we find

$$\frac{\frac{2}{\rho_o} \Delta T \left(\frac{\partial \varepsilon}{\partial T}\right)_{p,o} V^2 \left\{\frac{\eta}{1-\eta}\right\}^2}{K \nu} = 295$$

for convection to occur when the apparatus is not rotating.

The dimensions of the hypothetical experiment considered here are listed in Table IV.

Table IV

Dimensions of Hypothetical Experiment

Symbol	Term	Numerical Value
η	aspect ratio	0.40
R_i	inner radius	10 cm
R_o	outer radius	25 cm
a	annulus depth	15 cm
ΔT	temperature difference	5°C
e	ellipticity	0.05

The properties of the hypothetical working fluid used in this experiment are listed in Table V.

Table V

Properties of Hypothetical Working Fluid

Symbol	Term	Numerical Value	Reference
α	coef. of expan.	1.08×10^{-3} °C	1
$\left(\frac{\partial \varepsilon}{\partial T}\right)_{p,o}$	coef. of permit.	3.32×10^{-14} f/m-°C	1
K	th. diffusivity	6.40×10^{-8} m^2/s	2
ν	kin. viscosity	10^{-4} m^2/s	2
ρ	density	873 kg/m^3	2
ε_o	permittivity const.	8.854×10^{-12} f/m	3
ε	dielectric const.	2.60	1
C_p	sp. heat	1.9×10^3 j/kg°C	2

The references are : (1) Chandra and Smylie (1972); (2) Hart (1976); (3) Moore (1973).

From the definition of the Rayleigh number we find

$$V = 3.34 \text{ KV}$$

for convection to occur in the hypothetical apparatus ($\eta = 0.4$) without rotation and with a 5°C temperature contrast across the annulus. We note that with a thin annulus gap ($\eta = 0.8$) the voltage requirement is

$$V = 0.55 \text{ KV}$$

under the same operating conditions. To achieve Rayleigh numbers one order of magnitude larger than the critical Rayleigh number in the stationary apparatus requires

$$V = 10.5 \text{ KV for } \eta = 0.4$$

$V = 1.76$ KV for $\eta = 0.8$

The capacitance of the apparatus is given by

$$C = \frac{4 \pi \varepsilon R_i R_o}{a}$$

which is the capacitance of a spherical condenser (Moore, 1973). For the hypothetical experiment

$$C = 48.2 \times 10^{-12} \text{ farads}$$

The electrical energy stored in the experimental apparatus is given by (Moore, 1973)

$$w = 1/2\ CV^2$$

or

$$w = .003 \text{ watt-sec}$$

for a voltage of 10.5 KV.

For a rotation rate of 20 rpm the Eckman number is 7.64×10^{-4}. The rate of precession required to produce instability is calculated from equation (16) for an inclination of 30° between rotation and precession axes,

$$\Omega = .56 \text{ rpm}$$

Modeling the circuit needed to create the electric field as a one ohm resistance and capacitance of 48×10^{-12} f in series, the total impedance of the circuit is $5.50 \times 10^{7}\ \Omega$. The real power supplied by a 60 hz voltage supply of peak output 10.5 KV is then

$$P = 1.60 \times 10^{-3} \text{ watts.}$$

Heat flux by conduction is (Krieth, 1973)

$$q = \frac{4\pi R_i R_o k (T_o - T_i)}{a}$$

where k is the thermal conductivity. The fluid properties in Table II give a conductivity of $k = \kappa C_p \rho = 1.06 \times 10^{-1} \frac{\text{joules}}{°C\text{-m-s}}$ and the heat flux is thus

$$q = 1.11 \text{ watts}$$

for a temperature contrast of 5°C.

The total power demand on the laboratory is therefore on the order of 1 watt. To achieve Rayleigh numbers up to one order of magnitude greater than critical requires up to about 10 KV. At a rotation rate of 20 rpm, the empirical equation of Ma'kus (1968) predicts that a precession rate of 0.56 rpm is required to initiate instabilities.

CONCLUSION

A. Current Work

A well-defined experiment could be essential for providing the physical basis to evaluate and compare geodynamo driving mechanisms. Of particular interest is an experiment to evaluate the effect of stable thermal stratification and thermal convection on the precessional geodynamo model. In this work it is found that such an experiment is feasible in an apparatus consisting of a concentric inner sphere of 10 cm radius and an elliptical outer shell with major and minor radii of 25 cm and 24 cm, respectively, provided

(1) a potential of the order of 10 KV is maintained between the shells;

(2) a temperature difference of $5^{o}C$ is imposed across the annulus;

and

(3) the apparatus can be made to rotate and precess at rates of 20 rpm and 1 rpm, respectively, with a 30^{o} angle between the axis of rotation and the axis of precession.

B. Recommendations for Future Research

Besides the design, construction, and testing of the experimental apparatus important tasks which should be completed as soon as possible include:

(1) Inclusion of variable viscosity and the effect of rotation in the numerical model of convection presented here;

(2) Development of a numerical model of the precessional flow to verify the empirical equation of Malkus (1968) and to determine the effect of the inner core on the flow;

(3) Combination of the two numerical models to predict the results of the experiment and to verify the assumption that both convective and precessional flow instabilities will exist when the conditions generating them are present simultaneously.

REFERENCES

Busse, F.H. (1975a) A Necessary Condition for the Geodynamo. J Geophys Res, 80, 278-280.

Busse, F.H. (1975b) Core Motions and the Geodynamo. Rev Geophys Space Phys, 13, 206-241.

Busse, F.H. (1968) Steady Fluid Flow in a Precessing Spheroidal Shell, J Fluid Mech, 33, 739-751.

Chandra, B. and Smylie, D.E. (1972) A Laboratory Model of Thermal Convection Under a Central Force Field. Geophys Fluid Dyn, 3, 211-224.

Chandrasekhar, S. (1961) Hydrodynamic and Hydromagnetic Stability. Oxford University Press, New York.

Crandall, S.H. (1956) Engineering Analysis. McGraw-Hill Book Co, New York.

Durney, B. (1976) Private Communication.

Durney, B. (1970) Nonaxisymmetric Convection in a Rotating Spherical Shell. Astrophys J, 161, 1115-1127.

Durney, B. (1968a) Convective Spherical Shell: I. No Rotation. J Atmos Sci, 25, 372-380.

Durney, B. (1968b) Convective Spherical Shell: II. With Rotation. J Atmos Sci, 25, 771 ff.

Frazer, M.C. (1973) Temperature Gradients and the Convective Velocity in the Earth's Core. Geophys J Royal Astron Soc, 34, 193-201.

Gans, R.F. (1972) Viscosity of the Earth's Core, J of Geophys Res, 77, No. 2, 360-366.

Gilman, P. (1976) Private Communication.

Gilman, P.A. (1975) Linear Simulations of Boussinesq Convection in a Deep Rotating Spherical Shell. J Atmos Sci, 32, 1331-1352.

Gross, M.J. (1967) Laboratory Analogies for Convection Problems. Mantles of the Earth and Terrestrial Planets, S.K. Runcorn, ed. Interscience Publishers, New York.

Hart, J.E. (1976) Studies of Earth Simulation Experiments. Technical Report under NASA Contract # NAS8-31149.

Jacobs, J.A., Russell, R.D., and Wilson, J.T. (1974) Physics and Geology, 2nd Edition. McGraw-Hill Book Co, New York.

Kennedy, G.C. and Higgins, G.H. (1973) The Core Paradox, J Geophys Res, 78, 900-904.

Krieth, F. (1973) Principles of Heat Transfer, Third Edition. Intext Educational Publishers, New York.

Malkus, W.V.R. (1968) Precession of the Earth as the Casue of Geomagnetism. Science, 160, 3825, 259-264.

Moore, A.D. (1973) Electro-Statics and its Applications. John Wiley and Sons, New York.

Pickard, W.F. (1965) Electrical Force Effects in Dielectric Liquids. Progress in Dielectrics, 6, J.B. Birks and J. Hart, eds. Academic Press, Inc , New York.

Rochester, M.G., Jacobs, J.A., Smylie, D.E., and Chong, K.F. (1975). Can Precession Power the Geomagnetic Dynamo? J Royal Astro Soc, 43, 661-678.

Smylie, D.E. (1966) Thermal Convection in Dielectric Liquids and Modelling in Geophysical Fluid Dynamics. Earth and Planetary Sci Letters, 1, 339-340.

Smyth, C.P. (1955) Dielectric Behavior and Structure. McGraw-Hill Book Co, Inc, New York.

Young, C. Cox, Andrew, and Winn, C.Byron (1976) "Part B: Geodynamo Experiments," in Assessment of Geophysical Flows for Zero-Gravity Simulation, NASA Contract NAS8-31347 Progress Report, March 1976.

APPENDIX I

Computer Algorithm for the Eigenvalue Problem

Eigenvalue Algorithm

The algorithm described here solves eigenvalue problems of the form

$$\frac{d^6y}{dx^6} + c_1 \frac{d^5y}{dx^5} + c_2 \frac{d^4y}{dx^4} + c_3 \frac{d^3y}{dx^3} + c_4 \frac{d^2y}{dx^2} + c_5 \frac{dy}{dx} + c_6 y = \lambda c_7 y \qquad (1)$$

on the domain $\eta \leq x \leq \ell$, with the six boundary conditions

$$f_{11} \frac{d^4y}{dx^4} + f_{12} \frac{d^3y}{dx^3} + f_{13} \frac{d^2y}{dx^2} + f_{14} \frac{dy}{dx} + f_{15} y = 0 \qquad (2a)$$

$$f_{23} \frac{d^2y}{dx^2} + f_{24} \frac{dy}{dx} + f_{25} y = 0 \qquad (2b)$$

and

$$y = 0 \qquad (2c)$$

at $x = \eta, \ell$. λ is the eigenvalue and coefficients c_i and f_{ij} are functions of the independent variable x and wave number w.

The finite difference operators used to create the matrix equation equivalent of (1) and boundary conditions (2) are shown in Figure 8. The domain is modeled as a set of (n+6) nodes with n nodes on the interior of the domain, 4 nodes exterior to the domain and 1 node at each boundary (see figure below).

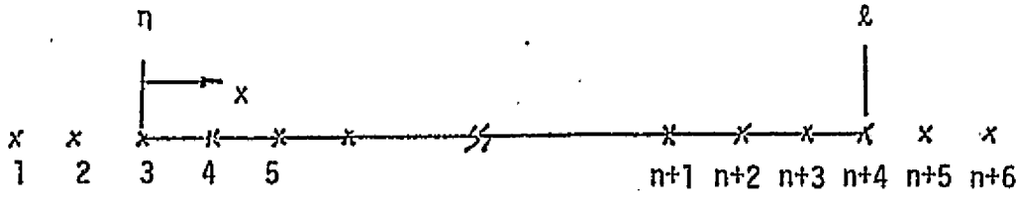

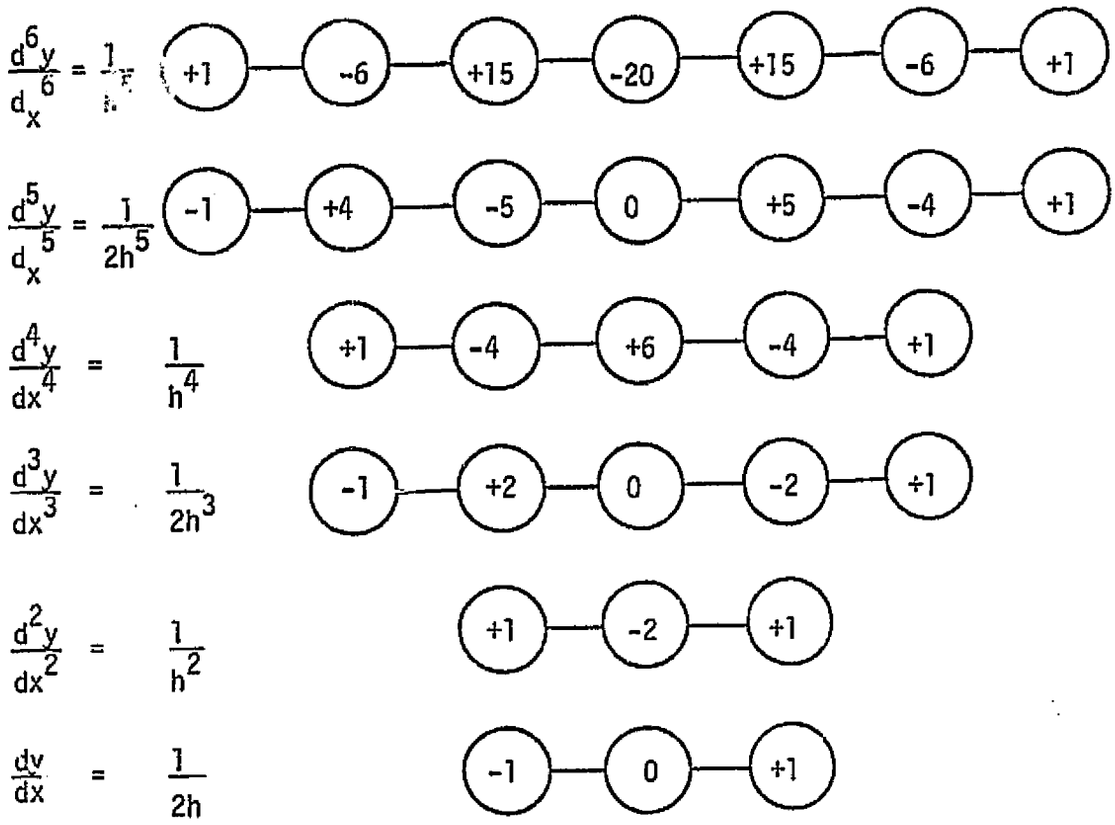

Figure 8. Finite difference computational molecules. h is the spacing between nodes.

At node i the finite difference equation representing (1) is

$$\left\{\frac{1}{h^6} - \frac{c_1}{2h^5}\right\} y_{i-3} - \left\{\frac{6}{h^6} - \frac{2c_1}{h^5} - \frac{c_2}{h^4} + \frac{c_3}{2h^3}\right\} y_{i-2}$$

$$+ \left\{\frac{15}{h^6} - \frac{2.5c_1}{h^5} - \frac{4c_2}{h^4} + \frac{c_3}{h^3} + \frac{c_4}{h^2} - \frac{c_5}{2h}\right\} y_{i-1}$$

$$- \left\{\frac{20}{h^6} - \frac{6c_2}{h^4} + \frac{2c_4}{h^2} - c_6\right\} y_i$$

$$+ \left\{\frac{15}{h^6} + \frac{2.5c_1}{h^5} - \frac{4c_2}{h^4} - \frac{c_3}{h_3} + \frac{c_4}{h^2} + \frac{c_5}{2h}\right\} y_{i+1}$$

$$- \left\{\frac{6}{h^6} + \frac{2c_1}{h^5} - \frac{c_2}{h^4} - \frac{c_3}{2h^3}\right\} y_{i+2} + \left\{\frac{1}{h^6} + \frac{c_1}{2h^5}\right\} y_{i+3} = c_7 \lambda y_i \qquad (3)$$

where h is the spacing between nodal points. Applying the finite difference operators across the domain and applying the boundary conditions puts the eigenvalue problem in standard matrix form,

$$[A] \{y\} = \lambda [B] \{y\}$$

in which [A] and [B] are n x n matrices and {y} is the n x 1 eigenvector. Off-diagonal elements of [B] are zero and [A] is a banded matrix with a bandwidth of 7.

By using the finite difference operators the boundary conditions must first be stated in the useful form

$$y_1 = BC(1,1)\, y_4 + BC(1,2)\, y_5 \qquad (4a)$$

and

$$y_2 = BC(2,1)\, y_4 + BC(2,2)\, y_5 \qquad (4b)$$

at the left end, and

$$y_1 = BC\ (3,1)\ y_i + BC\ (3,2)\ y_j \tag{4c}$$

and

$$y_m = BC\ (4,1)\ y_i + BC\ (4,2)\ y_j \tag{4d}$$

at the right end (see figure below).

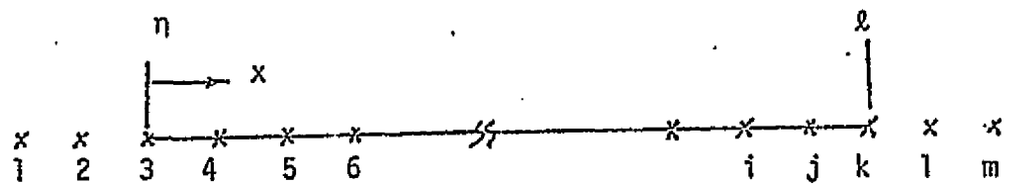

For example, writing the second-order boundary condition in finite difference form for the left end, we have

$$\left\{\frac{f_{23}}{h^2} - \frac{f_{24}}{2h}\right\}\ y_2 + \left\{\frac{f_{23}}{h^2} + \frac{f_{24}}{2h}\right\}\ y_4 = 0$$

where the coefficients f_{ij} are evaluated at $x = \eta$. Solving for y_2

$$y_2 = \left\{\frac{hf_{24} + 2f_{23}}{hf_{24} - 2f_{22}}\right\}\ y_4$$

and we have thus found

$$BC\ (1,1) = \frac{hf_{24} + 2f_{23}}{hf_{24} - 2f_{22}} \tag{5a}$$

and

$$BC\ (1,2) = 0.0 \tag{5b}$$

Writing the fourth-order boundary condition in finite-difference form at the left end, we have

$$\left\{\frac{f_{11}}{h^4} - \frac{f_{12}}{2h^3}\right\} y_1 - \left\{\frac{4f_{11}}{h^4} - \frac{f_{12}}{h^2} + \frac{f_{14}}{2h}\right\} y_2$$

$$- \left\{\frac{4f_{11}}{h^4} + \frac{f_{12}}{h^3} - \frac{f_{13}}{h^2} - \frac{f_{14}}{2h}\right\} y_4$$

$$+ \left\{\frac{f_{11}}{h^4} + \frac{f_{12}}{2h^3}\right\} y_5 = 0$$

where again the coefficients f_{ij} are evaluated at $x = \eta$. After solving for y_1 and noting that

$y_2 = BC\ (2,1)\ y_1$ we have

$$y_1 = \left\{(BC(2,1) + 1) \quad \frac{2h^2 f_{13} - 8f_{11}}{hf_{12} - 2f_{11}} + (BC(2,1) - 1) \quad \frac{2hf_{12} - h^3 f_{14}}{hf_{12} - 2f_{11}}\right\} y_4$$

$$+ \left\{\frac{hf_{12} + 2f_{11}}{hf_{12} - 2f_{11}}\right\} y_5$$

We have now found

$$BC\ (1,1) = (BC\ (2,1) + 1) \left\{\frac{2h^2 f_{13} - 8f_{11}}{hf_{12} - 2f_{11}}\right\} + (BC(2,1) - 1)\left\{\frac{2hf_{12} - h^3 f_{14}}{hf_{12} - 2f_{11}}\right\} \quad (5c)$$

and

$$BC\ (1,2) = \frac{hf_{12} + 2f_{11}}{hf_{12} - 2f_{11}} \quad (5d)$$

Similarly it can be shown that

$$BC\ (3,1) = 0.0 \quad (5e)$$

$$BC\ (3,2) = \frac{hf_{24} - 2f_{23}}{hf_{24} + 2f_{23}} \tag{5f}$$

$$BC\ (4,1) = \frac{hf_{12} - 2f_{11}}{hf_{12} + 2f_{11}} \tag{5g}$$

and

$$BC\ (4,2) = (BC\ (3,2) + 1)\left\{\frac{8f_{11} - 2h^2 f_{13}}{2f_{11} + hf_{12}}\right\} + (BC\ (3,2) - 1)$$

$$\left\{\frac{2hf_{12} - h^3 f_{14}}{hf_{12} + 2f_{11}}\right\} \tag{5h}$$

where coefficients $f_{i,\,j}$ are evaluated at $x = \ell$.

Now the matrix generated by equation (3) is an n by (n + 6) matrix which must be transformed to an n x n matrix through the application of the boundary conditions. With two interior nodal points, for example, eight nodal points are used to model the domain:

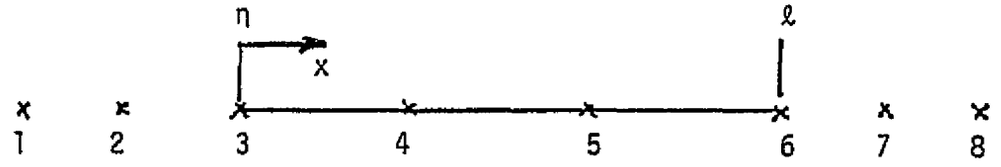

The resulting matrix equation formed by repeated application of (3) is

$$\begin{bmatrix} a_{11} & a_{12} & a_{13} & \cdots & a_{18} \\ a_{21} & a_{22} & a_{23} & \cdots & a_{28} \end{bmatrix} \begin{Bmatrix} y_1 \\ y_2 \\ \vdots \\ y_8 \end{Bmatrix} = \lambda \begin{bmatrix} b_{11} & b_{12} \\ b_{21} & b_{22} \end{bmatrix} \begin{Bmatrix} y_4 \\ y_5 \end{Bmatrix}$$

The boundary conditions are stated in the form

$$y_1 = BC\ (1,\ 1)\ y_4 + BC\ (1,\ 2)\ y_5$$

$$y_2 = BC\ (2,\ 1)\ y_4 + BC\ (2,\ 2)\ y_5$$

$$y_7 \quad BC\ (3,\ 1)\ y_5 + BC\ (3,\ 2)\ y_6$$

$$y_8 \quad BC\ (4,\ 1)\ y_5 + BC\ (4,\ 2)\ y_6$$

Substituting these into the matrix equation the eigenvalue problem becomes

$$\begin{bmatrix} a'_{14} & a'_{15} \\ a'_{24} & a'_{25} \end{bmatrix} \begin{Bmatrix} y_4 \\ y_5 \end{Bmatrix} = \lambda \begin{bmatrix} b_{11} & b_{12} \\ b_{21} & b_{22} \end{bmatrix} \begin{Bmatrix} y_4 \\ y_5 \end{Bmatrix}$$

where

$$a'_{14} = a_{14} + a_{11}\ BC\ (1,1) + a_{12}\ BC\ (2,1) + a_{17}\ BC\ (3,1) + a_{18}\ BC\ (4,1)$$

$$a'_{15} = a_{15} + a_{11}\ BC\ (1,2) + a_{12}\ BC\ (2,2) + a_{17}\ BC\ (3,2) + a_{18}\ BC\ (4,2)$$

$$a'_{24} = a_{24} + a_{21}\ BC\ (1,1) + a_{22}\ BC\ (2,1) + a_{27}\ BC\ (3,1) + a_{28}\ BC\ (4,1)$$

and

$$a'_{25} = a_{25} + a_{21}\ BC\ (1,2) + a_{22}\ BC\ (2,2) + a_{27}\ BC\ (3,2) + a_{28}\ BC\ (4,2)$$

At this stage the eigenvalue problem has been reduced to the form

$$[A]\ \{y\} = \lambda\ [B]\ \{y\}$$

which several readily available computer routines can solve.

For convenience, the International Mathematics and Statistics Library (IMSL) edition 5 routine EIGZF was used to solve the problem, once it had been put in the standard form. It should be noted that the matrix equation equivalent of equation (1) with boundary conditions (2) is not necessarily symmetric, requiring a sophisticated eigenvalue routine.

Subroutine EIGZF was found to work well for all cases and provided complex eigenvalues and eigenvectors. With only a few exceptions, the imaginary parts of both the eigenvalues and eigenvectors were zero.

Use of Program CONVECT

To solve a particular eigenvalue problem the user of program CONVECT must

1. punch cards with the coefficients of the governing equation c_i $i = 1, 7$, and insert them in subroutine COEFF;

2. punch cards with the coefficients f_{ij}, $i = 1, 2$, $j = 1, 4$, and insert them in subroutine BCOEFF; and

3. punch data card(s) with input values for

   ETA : left end of domain

   XF : right end of domain

   L : wave number

   NUMDIV: number of divisions of the domain

The data card(s) are punched in the format shown below:

L	NUMDIV	ETA	XF
(I10)	(I10)	(F10.4)	(F10.4)

The coefficients c_i are specified by assignment statements of the form

c(1) = c_1/2.0/DX5

c(2) c_2/DX4

c(3) c_3/2.0/DX3

$c(4) = c_4/DX2$

$c(5) = c_5/2.0/DX$

$c(6) = c_6$

and

$c(7) = c_7$

The coefficients f_{ij} are specified by statement functions of the form

$F_{11}(x,w)$, $F_{12}(x,w)$, etc.

where w is a wave number. Both arguments must be included, even if both are not used. On the printed output the program will provide, among other things, the eigenvalues and eigenvectors as complex numbers. A single eigenvalue or element of an eigenvector will appear as

(real part, imaginary part)

For the 35 x 35 matrices used to solve the critical Rayliegh number problem, central processor times of slightly less than 20 seconds were typical.

Verification of CONVECT

To verify the accuracy of the program, a sixth order eigenvalue problem for which one solution could be determined analytically was solved. The verification problem was[1]

$$\frac{d^6y}{dx^6} + k\frac{d^5y}{dx^5} + k^2\frac{d^4y}{dx^4} + k^3\frac{d^3y}{dx^3} + k^4\frac{d^2y}{dx^2} = -k^6y$$

with boundary conditions

$$y = \frac{d^2y}{dx^2} = 0 \text{ at } x = 0,\pi \quad \text{and} \quad \frac{d^3y}{dx^3} + k^2\frac{dy}{dx} = 0 \text{ at } x = 0,\pi$$

[1]This verification problem was suggested by Dr. Bernard Durney.

A particular solution of the equation is

$$y = A\sin kx + B\cos kx$$

After applying the boundary conditions the solution is reduced to

$$y = A\sin kx,\ k = 1, 2, 3, \ldots n$$

where k is the characteristic value and sin kx is the mode. The problem was put on the computer in the form

$$\frac{d^6y}{dx^6} + \frac{d^5y}{dx^5} + \frac{d^4y}{dx^4} + \frac{d^3y}{dx^3} + \frac{d^2y}{dx^2} = \lambda y$$

with the boundary conditions

$$y = \frac{d^2y}{dx^2} = 0 \quad \text{at } x = 0, \pi$$

and

$$\frac{d^3y}{dx^3} + \frac{dy}{dx} = 0 \text{ at } x = 0, \pi$$

Thus the critical (minimum) eigenvalue was expected to be

$$k = (-\lambda)^{1/6} = 1.0$$

and the mode $y = \sin x$. The results are plotted in Figure 9 and show good convergence. The convergence of the convection problem (see Chapter III) is shown in Figure 10. Some instability was present when fewer than four interior nodal points were used to model the domain, but these instabilities disappeared as the number of equations was increased and the solution converged to two significant figures at 35 equations.

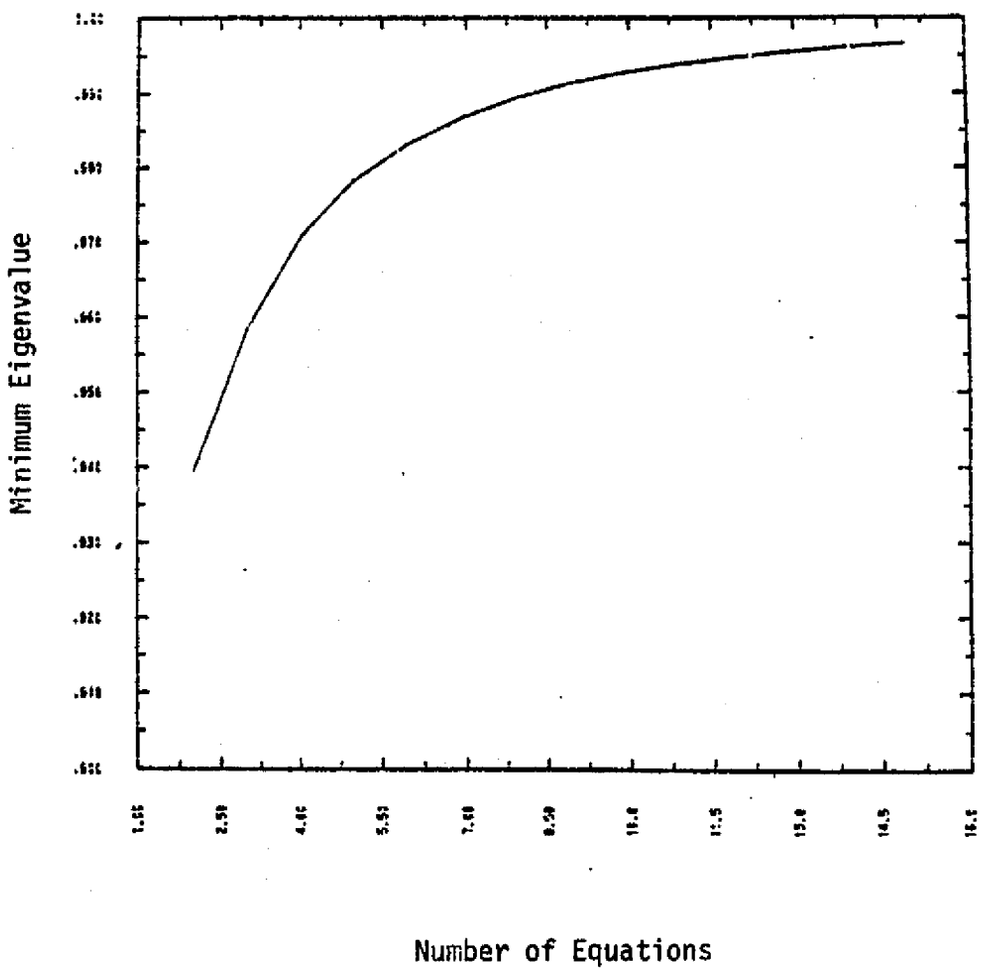

Figure 9a: Verification of CONVECT: Convergence of Eigenvalue. After 10 equations the solution has converged to within 1% of 1.00, the exact solution.

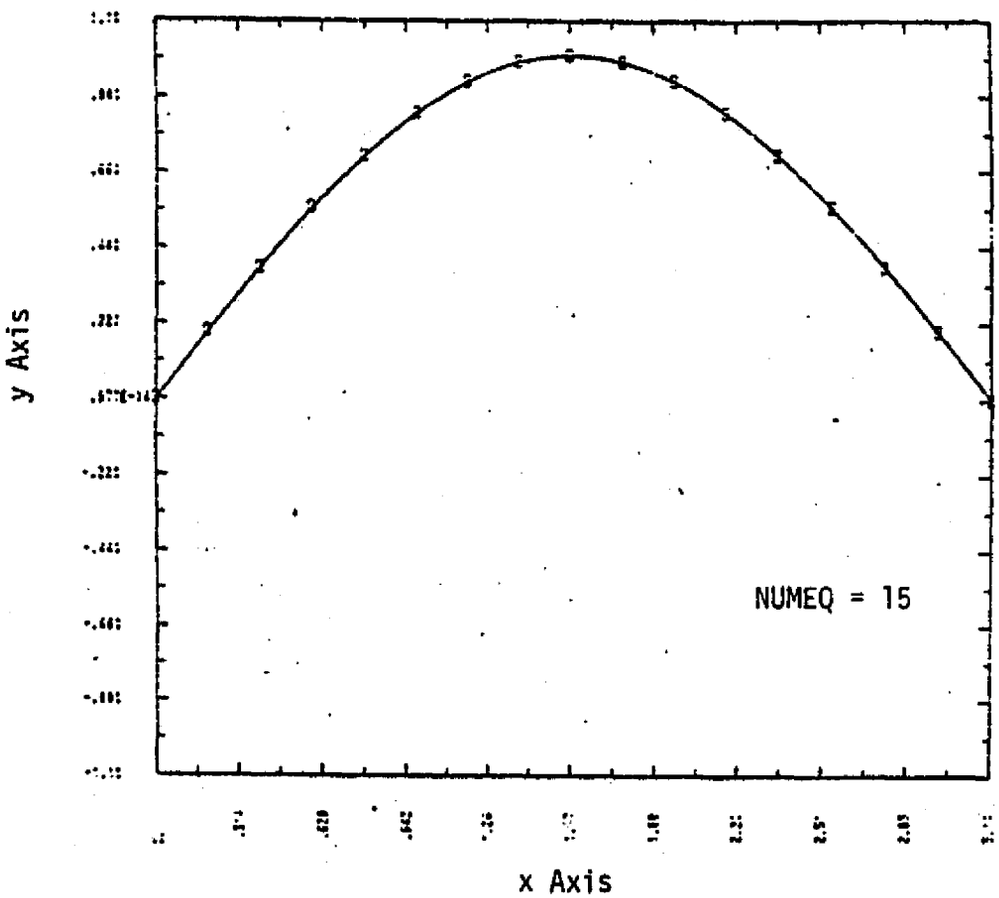

Figure 9b: Verification of CONVECT Convergence of Mode. Solid line is a plot of sin x for $0 \leq x \leq \pi$ and is the exact solution to the eigenvalue problem. The squares are the elements of the eigenvector computed by program CONVECT The figure shows good agreement between exact and computer solutions.

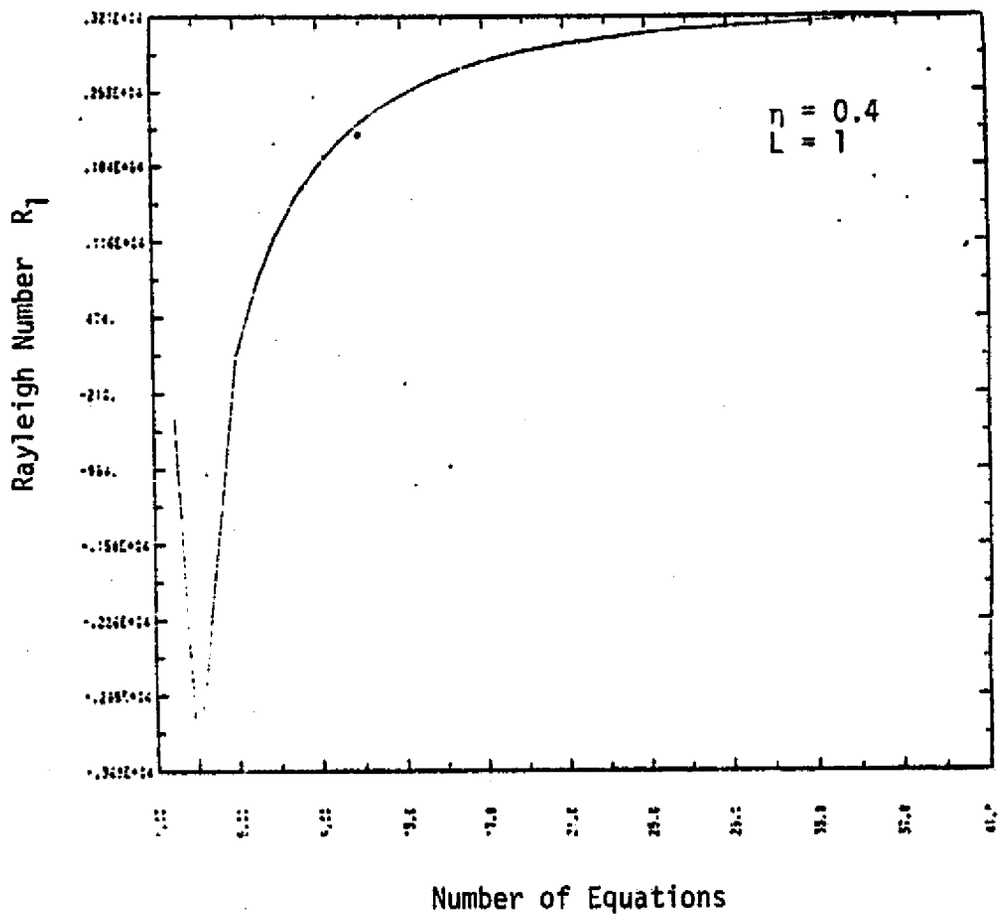

Figure 10. Convergence of Rayleigh Number. Solution of annulus problem is plotted for up to 40 equations. Some instability is present with less than 4 equations. 35 equations were used in the numerical solution described in Chapter III.

APPENDIX II

Program Listing and Sample Output

Included in this appendix is a listing of program CONVECT and sample output. The output is for the rigid boundary annulus problem with L = 1, η = 0.4, and NUMEQ = 10. The first two pages of output describe the formulation of the problem, ending on the second page with the matrices A and B ready for input to the eigenvalue routine. On the third page the solution of the eigenvalue problem is printed, with eigenvalues representing the Rayleigh number R_1 and eigenvector representing the temperature variable θ. θ is arbitrarily normalized so its largest element is unity. The minimum eigenvalue is R_1 = 2063.01 or, equivalently, $R_a = (.6)^3 R_1 = 446$. The corresponding mode is

.556

.875

1.00

.988

.890

.746

.583

.420

.265

.125

```
      PROGRAM CONVEC
     *(INPUT,OUTPUT,TAPE5=INPUT,TAPE6=OUTPUT)


C     USING THE FINITE-DIFFERENCE METHOD, THIS PROGRAM SOLVES A ONE-
C     DIMENSIONAL, SIXTH-ORDER EIGENVALUE PROBLEM WITH TWO ZERO ORDER,
C     TWO SECOND ORDER AND TWO FOURTH ORDER BOUNDARY CONDITIONS.
C     FURTHER DOCUMENTATION IS TO BE FOUND IN
C
C       COX, S.L. (1976) FEASIBILITY OF A ZERO GRAVITY GEODYNAMO
C            EXPERIMENT, MSC THESIS, DEPARTMENT OF MECHANICAL
C            ENGINEERING, COLORADO STATE UNIVERSITY,  FORT COLLINS
C            COLORADO
C
C     NOTE-- THE USER MUST SUPPLY THE COEFFICIENTS OF THE EQUATION
C     AND THE BOUNDARY CONDITIONS IN SUBROUTINES COEFF AND BCOEFF,
C     RESPECTIVELY.  IMPORTANT VARIABLES IN THE PROGRAM ARE
C
C       ON INPUT
C
C         L         WAVE NUMBER
C         NUMDIV    NUMBER OF DIVISIONS OF DOMAIN
C         ETA       COORDINATE OF LEFT END OF DOMAIN
C         XF        COORDINATE OF RIGHT END OF DOMAIN
C
C       ON OUTPUT (TO SUBROUTINE EIGEN)
C
C         NUMEQ     NUMBER OF EQUATIONS
C         AST(I,J)  MATRIX A OF STANDARD-FORM EIGENVALUE PROBLEM
C         B(I,J)    ASSOCIATED MATRIX B OF EIGENVALUE PROBLEM
C
C       DURING EXECUTION
C
C         X         POSITION OF NODE
C         DX        SPACING BETWEEN NODES
C         C(I)      COEFFICIENTS OF GOVERNING EQUATION
C         BC(I,J)   BOUNDARY CONDITION MATRIX
C         RHS(I)    RIGHT-HAND SIDE OF EQUATION I
C         IER       ERROR PARAMETER FROM ROUTINE EIGZF
C         A    (I,J) NUMEQ BY (NUMEQ+6) MATRIX OF GOVERNING EQUATION
C         RL1       REAL REPRESENTATION OF WAVE NUMBER L1


      COMMON/COEF/
     *ETA,XF,A,DX,RL1

      COMMON/EIGENV/
     *AST(35,35),B(35,35)

      DIMENSION
     *A(41,41),RHS(35),BC(4,2),C(7)


C     READ AND CHECK INPUT DATA

   35 CONTINUE
      READ(5,2) L,NUMDIV,ETA,XF
      IF(EOF(5)) 1200,40
   40 CONTINUE
```

```
      WRITE(6,1)
      WRITE(6,2) L,NUMDIV,ETA,XF
C
C     INITIALIZE
C
      IPAGE=1
      LINE=5
      X=ETA
      DX=(XF-ETA)/FLOAT(NUMDIV)
      DX6=DX**6.0
      L1=(L+1)*L
      FL1=FLOAT(L1)
      DO 50 I=1,41
      DO 50 J=1,41
      A(I,J)=0.0
   50 CONTINUE
      NUMEQ=NUMDIV-1
      DO 100 I=1,NUMEQ
      DO 100 J=1,NUMEQ
      AST3(I,J)=0.0
  100 CONTINUE
C
C     FORMULATE THE A MATRIX
C
      IEND=NUMDIV+2
      DO 200 I=4,IEND
C
      X=X+DX
      CALL COEFF(C)
C
      A(I-3,I-3)=+1.0/DX6-C(1)
      A(I-3,I-2)=-6.0/DX6+4.0*C(1)+C(2)-C(3)
      A(I-3,I-1)=+15.0/DX6-5.0*C(1)-4.0*C(2)+2.0*C(3)+C(4)-C(5)
      A(I-3,I)=-20.0/DX6+6.0*C(2)-2.0*C(4)+C(6)
      A(I-3,I+1)=+15.0/DX6+5.0*C(1)-4.0*C(2)-2.0*C(3)+C(4)+C(5)
      A(I-3,I+2)=-6.0/DX6-4.0*C(1)+C(2)+C(3)
      A(I-3,I+3)=+1.0/DX6+C(1)
      RHS(I-3)=C(7)
C
  200 CONTINUE
C
      IF(LINE .GE. (56-NUMEQ)) CALL NWPG(IPAGE,LINE)
      WRITE(6,6)
      DO 600 I=1,NUMEQ
      JEND=NUMDIV+5
      WRITE(6,5) (A(I,J),J=1,JEND)
      WRITE(6,14)
      LINE=LINE+3
  600 CONTINUE
C
      WRITE(6,7)
      WRITE(6,5) (RHS(I),I=1,NUMEQ)
      LINE=LINE+2
C
C     MODIFY THE A MATRIX TO ACCOUNT
C     FOR BOUNDARY CONDITIONS
```

```
C
      CALL BCOEFF(BC)
      IF(LINE .GT. 54) CALL NWPG(IPAGE,LINE)
      WRITE(6,3)
      WRITE(6,4) ((BC(I,J),J=1,2),I=1,4)
      LINE=LINE+4
      DO 300 I=1,NUMEQ
C
C     LEFT END
      A(I,4)=A(I,4)+A(I,1)*BC(1,1)+A(I,2)*BC(2,1)
      A(I,5)=A(I,5)+A(I,1)*BC(1,2)+A(I,2)*BC(2,2)
C
C     RIGHT END
      A(I,NUMDIV+1)=A(I,NUMDIV+1)+A(I,NUMDIV+4)*BC(3,1)
     1+A(I,NUMDIV+5)*BC(4,1)
      A(I,NUMDIV+2)=A(I,NUMDIV+2)+A(I,NUMDIV+4)*BC(3,2)
     1+A(I,NUMDIV+5)*BC(4,2)
  300 CONTINUE
C
C
C     DISCARD UN-NEEDED ELEMENTS OF THE MATRIX A.
C
      JEND=NUMDIV+2
      DO 500 I=1,NUMEQ
      DO 500 J=4,JEND
C
      JM3=J-3
      ASTD(I,JM3)=A(I,J)
C
  500 CONTINUE
C
      IF(LINE .GE. (58-2*NUMEQ)) CALL NWPG(IPAGE,LINE)
      WRITE(6,3)
      DO 700 I=1,NUMEQ
      WRITE(6,5) (ASTD(I,J),J=1,NUMEQ)
      WRITE(6,14)
      LINE=LINE+3
  700 CONTINUE
C
C
C     GENERATE B MATRIX FROM RHS
C
      IF(LINE .GE. (54-NUMEQ)) CALL NWPG(IPAGE,LINE)
      WRITE(6,9)
      DO 900 I=1,NUMEQ
      DO 800 J=1,NUMEQ
      B(I,J)=0.0
  800 CONTINUE
C
      B(I,I)=RHS(I)
      WRITE(6,5) (B(I,J),J=1,NUMEQ)
C
  900 CONTINUE
      LINE=LINE+NUMEQ
C
C
C     COMPUTE EIGENVALUES AND EIGENVECTORS AND PRINT OUT RESULT
C
      CALL EIGEN(NUMEQ)
```

```
C
      GO TO 33
C
 1200 CONTINUE
C
      STOP
C
    1 FORMAT(1H1,2X,*THE EIGENVALUE PROBLEM IS FORMULATED WITH*,//,40H
     1         L     NUMDIV        ETA          XF)
    2 FORMAT(2I10,2F10.4)
    3 FORMAT(/,10X,*BOUNDARY CONDITION MATRIX*)
    4 FORMAT(3(2E10.3,/),2E10.3)
    5 FORMAT(12E10.3)
    6 FORMAT(/,10X,*A MATRIX BEFORE REDUCTION*)
    7 FORMAT(/,10X,*RHS*)
    8 FORMAT(/,2X,*A MATRIX WITH BOUNDARY CONDITIONS*)
    9 FORMAT(/,2X,*S MATRIX*)
   14 FORMAT(1H )
C
      END
```

```
      SUBROUTINE NWPG(PAGE,LINE)
      INTEGER PAGE,LINE
C
C     THIS SUBROUTINE ADVANCES PRINTER TO NEW PAGE
C
      LINE=1
      PAGE=PAGE+1
      WRITE(6,1) PAGE
    1 FORMAT(1H1,120X,5HPAGE ,I3)
      RETURN
      END
```

```
      SUBROUTINE COEFF(C)
C
C     THIS ROUTINE CALCULATES THE COEFFICIENTS OF THE GOVERNING
C     EQUATION.  USER MUST SUPPLY STATEMENTS C(1) THROUGH C(7).
      COMMON/COEF/
     *ETA,XF,X,DX,RL1
C
      REAL C(7)
C
      DX2=DX*DX
      DX3=DX2*DX
      DX4=DX2*DX2
      DX5=DX4*DX
C
      C(1)=+10.0/X/2.0/DX5
      C(2)=+(96.0-3.0*RL1)/(X**2)/DX4
      C(3)=+(168.0-24.0*RL1)/(X**3)/2.0/DX3
      C(4)=+(3.0*RL1**2-42.0*RL1+72.0)/(X**4)/DX2
      C(5)=+(6.0*RL1**2-12.0*RL1)/(X**5)/2.0/DX
      C(6)=-(RL1**3-2.0*RL1**2)/(X**6)
      C(7)=-RL1*ETA/(ETA-1.0)/X**8
C
      RETURN
      END
```

```
      SUBROUTINE BCOEFF(BC)
C
C     THIS SUBROUTINE GENERATES THE BOUNDARY CONDITION MATRIX.  USER MUST
C     SUPPLY STATEMENT FUNCTIONS F11(X,W) THROUGH F24(X,W).
C
C
      COMMON/COEF/
     +ETA,XF,X,DX,RL1
C
      REAL BC(4,2)
C
      F11(X,W)=0.0
      F12(X,W)=+1.0
      F13(X,W)=+6.0/X
      F14(X,W)=+(0.0-W)/X**2
      F21(X,W)=0.0
      F22(X,W)=0.0
      F23(X,W)=+1.0
      F24(X,W)=+2.0/X
C
      DX2=DX**2
      DX3=DX**3
C
      BC(2,1)=(DX*F24(ETA,RL1)+2.0*F23(ETA,RL1))/
     +        (DX*F24(ETA,RL1)-2.0*F23(ETA,RL1))
      BC(2,2)=0.0
      BC(3,1)=0.0
      BC(3,2)=(DX*F24(XF,RL1)-2.0*F23(XF,RL1))/
     +        (DX*F24(XF,RL1)+2.0*F23(XF,RL1))
      BC(1,1)=(BC(2,1)+1.0)*(2.0*DX2*F13(ETA,RL1)-4.0*F11(ETA,RL1))/
     +        (DX*F12(ETA,RL1)-2.0*F11(ETA,RL1))
     +        +(BC(2,1)-1.0)*(2.0*DX*F12(ETA,RL1)-DX3*F14(ETA,RL1))/
     +        (DX*F12(ETA,RL1)-2.0*F11(ETA,RL1))
      BC(1,2)=(DX*F12(ETA,RL1)+2.0*F11(ETA,RL1))/
     +        (DX*F12(ETA,RL1)-2.0*F11(ETA,RL1))
      BC(4,1)=(DX*F12(XF,RL1)-2.0*F11(XF,RL1))/
     +(DX*F12(XF,RL1)+2.0*F11(XF,RL1))
      BC(4,2)=(BC(3,2)+1.0)*(6.0*F11(XF,RL1)-2.0*DX2*F13(XF,RL1))/
     +        (2.0*F11(XF,RL1)+DX*F12(XF,RL1))
     +        +(BC(3,2)-1.0)*(2.0*DX*F12(XF,RL1)-DX3*F14(XF,RL1))/
     +        (DX*F12(XF,RL1)+2.0*F11(XF,RL1))
C
      RETURN
      END
```

```
      SUBROUTINE EIGEN(NUMEQ)
C
C     THIS SUBROUTINE CALLS THE IMSL EDITION 5 ROUTINE EIGZF TO COMPUTE
C     THE EIGENVALUES AND EIGENVECTORS OF MATRIX A AND MATRIX B.
C
      COMMON/EIGENV/ '
     *A(35,35),B(35,35)
C
      REAL A,B
C
      COMPLEX
     *ALFA(35),LAMBDA(35),Z(35,35)
C
      REAL
     *BETA(35),WK(2500)
C
      WRITE(6,1)
      WRITE(6,2) NUMEQ
C
C
      CALL EIGZF(A,35,2,35,NUMEQ,2,ALFA,BETA,Z,35,WK,IER)
C
      IF(WK(1) .LT. 1.0) PRFRM=10HWELL
      IF(WK(1) .GT. 1.0 .AND. WK(1) .LT. 100.0) PRFRM=10HSATISFACTLY
      IF(WK(1) .GT. 100.0) PRFRM=10HPOORLY
      WRITE(6,6) PRFRM
      WRITE(6,10) IER
C
      DO 200 I=1,NUMEQ
  200   LAMBDA(I)=ALFA(I)/BETA(I)
      WRITE(6,7)
      WRITE(6,8) (LAMBDA(I),I=1,NUMEQ)
      WRITE(6,9)
      DO 300 I=1,NUMEQ
        WRITE(6,8) (Z(I,J),J=1,NUMEQ)
  300   WRITE(6,3)
C
    1 FORMAT(1H1,39H  THE EIGENVALUE PROBLEM IS SOLVED WITH,/,/,1H
     *,NUMEQ)
    2 FORMAT(I10)
    3 FORMAT(1H )
    6 FORMAT(1H0,34H  NOTE-- THE ALGORITHM HAS WORKED ,A10)
    7 FORMAT(1H0,43H  EIGENVALUES LAMBDA(1) ... LAMBDA(NUMEQ) ARE)
    8 FORMAT(4(1H(,E12.6,1H,,E12.6,1H)))
    9 FORMAT(1H0,39H  EIGENVECTORS ARE SUCCESIVE COLUMNS OF)
   10 FORMAT(1H0,10X,6HIER = ,I3)
C
      RETURN
      END
```

THE EIGENVALUE PROBLEM IS FORMULATED WITH

K	NO. OF EV	ETA	XF
1	11	.4000	1.0000

A MATRIX BEFORE REDUCTION

-.334E+07	-.145E+04	.174E+05	-.464E+05	.570E+03	-.339E+04	.730E+04	0.	0.	0.	0.	0.
0.	0.	0.	0.								
0.	.136E+07	-.444E+04	.245E+05	-.524E+03	.590E+03	-.332E+04	.746E+04	0.	0.	0.	0.
0.	0.	0.	0.								
0.	0.	.491E+07	-.650E+04	.280E+05	-.567E+03	.603E+03	-.329E+04	.714E+04	0.	0.	0.
0.	0.	0.	0.								
0.	0.	0.	.762E+07	-.822E+04	.316E+05	-.603E+03	.611E+03	-.323E+03	.681E+04	0.	0.
0.	0.	0.	0.								
0.	0.	0.	0.	.103E+04	-.957E+04	.344E+05	-.625E+03	.610E+03	-.315E+03	.657E+04	0.
0.	0.	0.	0.								
0.	0.	0.	0.	0.	.123E+04	-.117E+05	.380E+03	-.644E+03	.619E+03	-.312E+03	.636E+04
0.	0.	0.	0.								
0.	0.	0.	0.	0.	0.	.141E+04	-.117E+05	.385E+03	-.660E+03	.621E+03	-.308E+03
.618E+04	0.	0.	0.								
0.	0.	0.	0.	0.	0.	0.	.157E+04	-.119E+05	.401E+03	-.672E+03	.622E+03
-.302E+03	.613E+04	0.	0.								
0.	0.	0.	0.	0.	0.	0.	0.	.173E+04	-.132E+05	.415E+03	-.683E+03
.622E+03	-.295E+04	.594E+04	0.								
0.	0.	0.	0.	0.	0.	0.	0.	0.	.183E+04	-.136E+05	.420E+03
-.691E+03	.622E+03	-.295E+03	.577E+04								

EIGENVALUES

-.732E+05	-.254E+04	-.181E+03	-.635E+02	-.316E+02	-.178E+02	-.955E+01	-.557E+01	-.336E+01	-.209E+01	

BOUNDARY CONDITION MATRIX

-.498E+01	.153E+01	
-.132E+01	0.	
0.	-.697E+03	
.133E+01	-.3[illegible]E+01	

A MATRIX WITH HOMOGENEOUS BOUNDARY CONDITIONS

-.625E+05	.567E+05	-.733E+03	.795E+08	0.	0.	0.	0.	0.	0.
.233E+03	-.524E+03	.553E+09	-.382E+09	.746E+08	0.	0.	0.	0.	0.
-.656E+04	.248E+04	-.967E+09	.603E+09	-.320E+09	.712E+08	0.	0.	0.	0.
.742E+07	-.822E+08	.316E+03	-.601E+09	.611E+09	-.320E+09	.681E+08	0.	0.	0.
0.	.103E+08	-.957E+05	.344E+09	-.625E+09	.616E+09	-.315E+09	.857E+08	0.	0.
0.	0.	.123E+08	-.137E+09	.366E+09	-.644E+09	.619E+09	-.313E+09	.853E+08	0.
0.	0.	0.	.141E+08	-.117E+09	.385E+09	-.663E+09	.621E+09	-.33uE+09	.818E+08
0.	0.	0.	0.	.157E+08	-.225E+09	.431E+09	-.672E+09	.622E+09	-.382E+09
0.	0.	0.	0.	0.	.173E+08	-.132E+09	.415E+09	-.663E+09	.569E+09
0.	0.	0.	0.	0.	0.	.143E+08	-.134E+09	.484E+09	-.646E+09

U MATRIX

-.732E+03	0.	0.	0.	0.	0.	0.	0.	0.	0.
0.	-.249E+03	0.	0.	0.	0.	0.	0.	0.	0.
0.	0.	-.131E+03	0.	0.	0.	0.	0.	0.	0.
0.	0.	0.	-.625E+02	0.	0.	0.	0.	0.	0.
0.	0.	0.	0.	-.316E+02	0.	0.	0.	0.	0.
0.	0.	0.	0.	0.	-.178E+02	0.	0.	0.	0.
0.	0.	0.	0.	0.	0.	-.995E+01	0.	0.	0.
0.	0.	0.	0.	0.	0.	0.	-.557E+01	0.	0.
0.	0.	0.	0.	0.	0.	0.	0.	-.33uE+01	0.
0.	0.	0.	0.	0.	0.	0.	0.	0.	-.209E+01

```
THE EIGENVALUE PROBLEM IS SOLVED WITH

  RUPEC
     11

NOTE-- THE ALGORITHM HAS WORKED WELL

         IER =    0

   EIGENVALUES LAMBDA(1) ... LAMBDA(NUMEQ) ARE
( .[illegible]E+03,0.   )( .[illegible]E+03,0.   )( .242248E+06,0.   )( .631540E+08,0.   )
( .3637[illegible]E+07,0.   )( .425777E+07,0.   )( .313450E+06,0.   )( .117453E+07,0.   )
( .[illegible]E+04,0.   )( .454719E+05,0.   )(

   EIGENVECTORS ARE SUCCESSIVE COLUMNS OF
(-.2[illegible]E-04,0.   )(-.216763E-06,0.   )( .125137E-01,0.   )(-.334233E-03,0.   )
(-.[illegible]E+03,0.   )(-.961[illegible]E-01,0.   )( .100000E+01,0.   )(-.939724E+00,0.   )
( .556274E+03,0.   )(-.356542E+00,0.   )(

( .4[illegible]E-03,0.   )( .456[illegible]E-05,0.   )(-.797934E-01,0.   )( .848158E-02,0.   )
( .100000E+01,0.   )( .[illegible]E+00,0.   )(-.186627E-01,0.   )( .100000E+01,0.   )
( .875[illegible]E+00,0.   )(-.452722E+00,0.   )(

(-.[illegible]E-02,0.   )(-.[illegible]E-04,0.   )( .321734E+00,0.   )(-.537066E-01,0.   )
(-.[illegible]E+00,0.   )(-.[illegible]E+00,0.   )(-.747116E+00,0.   )( .340000E+00,0.   )
( .100000E+01,0.   )(-.231170E+00,0.   )(

( .28[illegible]E-01,0.   )( .76[illegible]E-04,0.   )(-.786623E+00,0.   )( .227185E+00,0.   )
(-.345415E+00,0.   )( .367[illegible]E+00,0.   )(-.661201E+00,0.   )(-.733131E+00,0.   )
( .[illegible]E+00,0.   )( .614370E+00,0.   )(

(-.124373E+00,0.   )(-.544724E-02,0.   )( .100000E+01,0.   )(-.622[illegible]E+00,0.   )
( .73[illegible]E+00,0.   )( .151[illegible]E+00,0.   )(-.774840E-03,0.   )(-.742059E+00,0.   )
( .[illegible]E+00,0.   )( .[illegible]E+00,0.   )(

( .402[illegible]E+00,0.   )( .[illegible]E-01,0.   )(-.184522E+00,0.   )( .100000E+01,0.   )
( .[illegible]E+00,0.   )(-.[illegible]E+00,0.   )( .559736E+00,0.   )(-.[illegible]E-02,0.   )
( .74[illegible]E+00,0.   )( .[illegible]E+01,0.   )(

(-.4[illegible]E+00,0.   )(-.127[illegible]E+00,0.   )(-.831471E+00,0.   )(-.621591E+00,0.   )
(-.245[illegible]E+00,0.   )(-.377[illegible]E+00,0.   )( .327755E+00,0.   )( .[illegible]E+00,0.   )
( .543295E+00,0.   )( .[illegible]E+00,0.   )(

( .1[illegible]E+01,0.   )( .374172E+00,0.   )( .135143E+00,0.   )(-.510302E+00,0.   )
(-.[illegible]E+00,0.   )( .[illegible]E+00,0.   )( .601045E+00,0.   )( .[illegible]E+00,0.   )
( .41[illegible]E+00,0.   )( .74[illegible]E+00,0.   )(

(-.247413E+00,0.   )(-.750[illegible]E+00,0.   )( .929421E+00,0.   )( .752815E+00,0.   )
(-.946417E+00,0.   )( .100000E+01,0.   )( .586626E+00,0.   )( .835687E+00,0.   )
( .265334E+00,0.   )( .456[illegible]E+00,0.   )(

(-.9951[illegible]E+00,0.   )( .100000E+01,0.   )( .696174E+00,0.   )( .820197E+00,0.   )
(-.524046E+00,0.   )( .[illegible]E+00,0.   )( .246610E+00,0.   )( .[illegible]E+00,0.   )
( .125219E+00,0.   )( .238123E+00,0.   )(
```

APPENDIX III

Free Surface Boundary Conditions

Free-surface boundary conditions on temperature are identical to rigid surface boundary conditions for temperature. Velocity boundary conditions for rigid surfaces are (Durney, 1968a)

$$P_L = P_L'' = 0 \quad \text{at } r = \eta, 1.$$

From equation 10(c) we find the equivalent conditions

$$D_L \theta_L = 0 \quad \text{at } r = \eta, 1$$

and

$$\frac{d^2}{dr^2} [r^3 D_L \theta_L] = 0 \text{ at } r = \eta, 1$$

By inserting the definition of the operator D_L these conditions can be written

$$\frac{d^4 \theta_L}{dr^4} + \frac{8}{r} \frac{d^3\theta_L}{dr^3} + \frac{(14 - L_1)}{r^2} \frac{d^2\theta_L}{dr^2}$$

$$+ \frac{4-2L_1}{r^3} \frac{d\theta_L}{dr} = 0 \quad \text{at } r = \eta, 1$$

and

$$\frac{d^2\theta_L}{dr^2} + \frac{2}{r} \frac{d\theta_L}{dr} - \frac{L_1}{r^2} \theta_L = 0 \quad \text{at } r = \eta, 1.$$

The mode of the free surface solution for wave number L = 3 is shown in Figure 11.

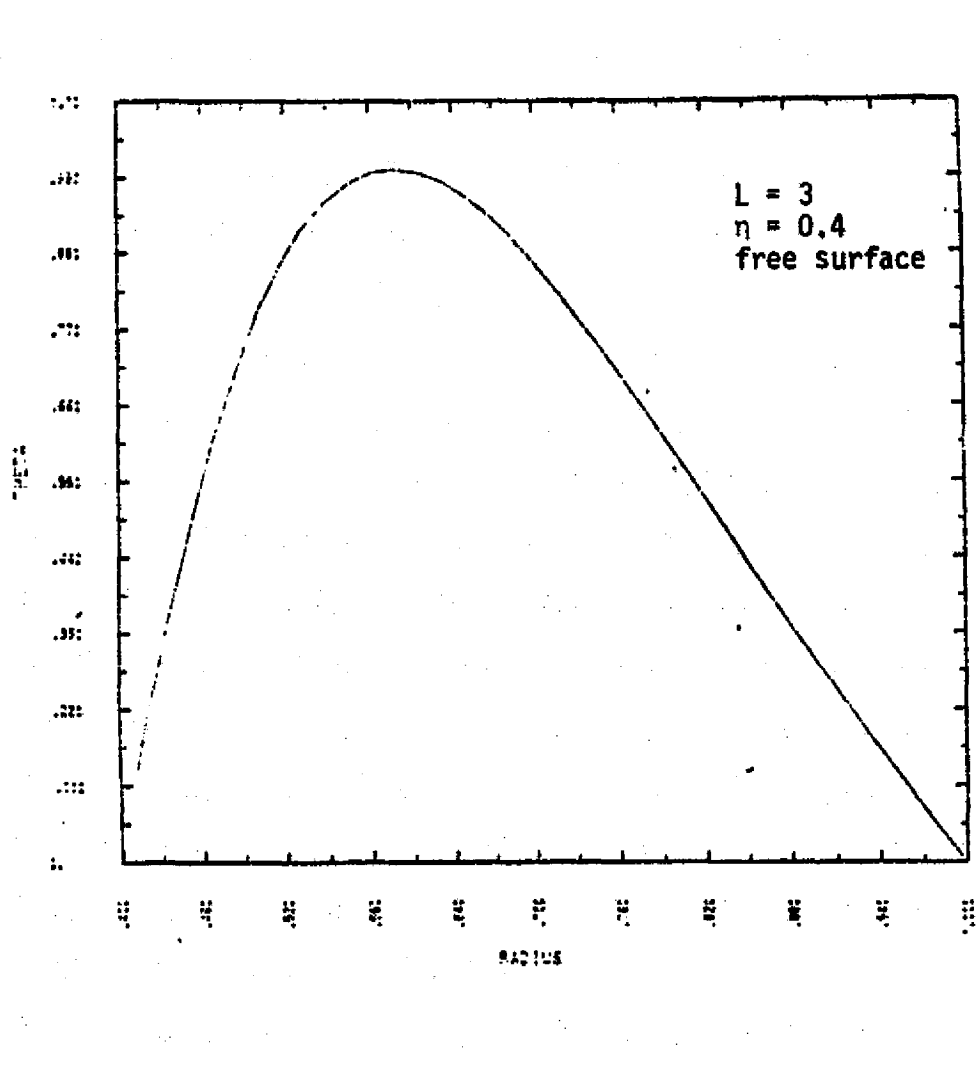

Figure 11a. Free Surface Solution: Mode Plot shows θ_L, L = 3, from inner annulus boundary to outer annulus boundary. θ_L is arbitrarily normalized so that its largest element is unity.

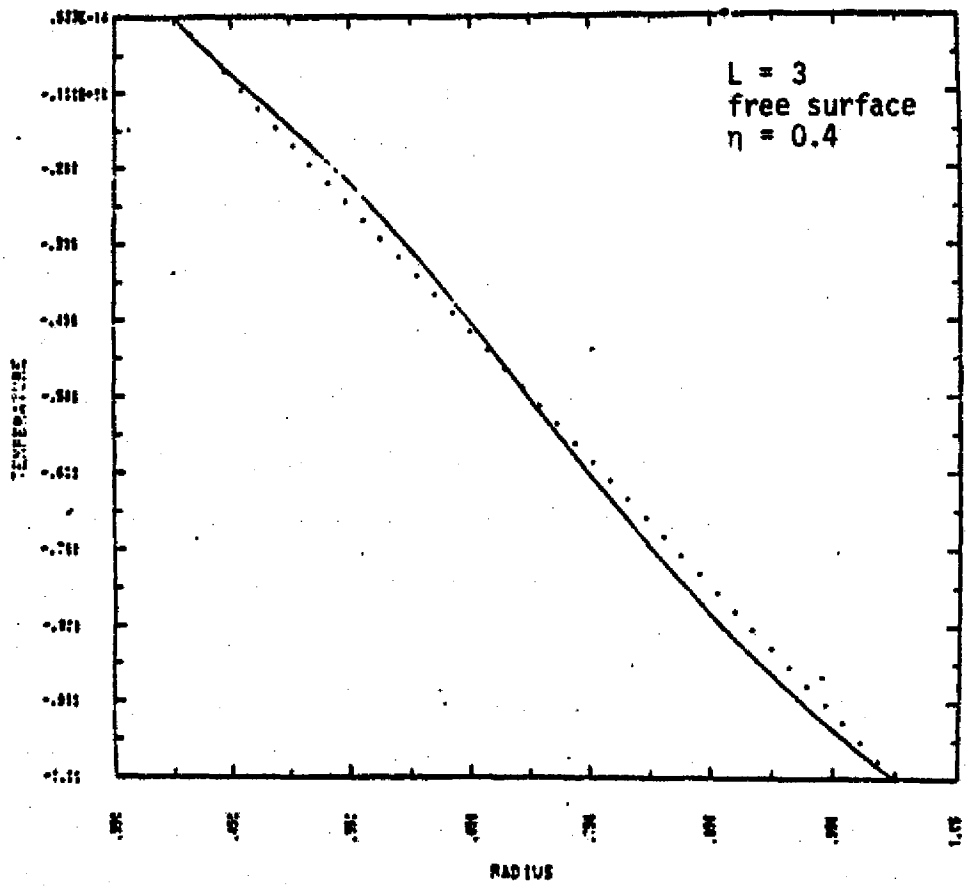

Figure 11b: Free Surface Solution: Temperature Profile. Dotted line is temperature profile of pure conduction, solid line shows sum of eigenvector θ_L, L = 3, and conduction profile. θ_3 has been arbitrarily normalized so its length is unity.

THERMO- HYDRO-DYNAMIC CHARACTERISTICS OF A ZERO-GRAVITY, SPHERICAL MODEL OF THE TROPOSPHERE

S. Srivatsangam
Research Associate
Dept. of Atmospheric Science
Colorado State University
Fort Collins, Colo. 80523

... authors

ABSTRACT

A model that exploits the radial inertia forces of a rotating fluid contained in a spherical annulus is described. The model would be flown in a satellite and experiments would be performed in very low or zero gravity. In such a model it would not be necessary to artificially simulate a radial gravity field. Thus small amounts of electrical energy would be sufficient to perform experiments. Since the only forces involved are thermo- hydro-dynamic ones, electromagnetic equations need not be considered.

INTRODUCTION

A variety of experiments have been performed under usual laboratory conditions to simulate the large-scale dynamics of the earth's atmosphere[3]. Of these the most successful so far are the cylindrical annulus experiments in which a liquid is confined between two concentric circular cylinders[9]. A radial thermal gradient -- resembling the meridional temperature variation in the atmosphere -- is imposed. Cameras are attached to record motions at different levels in the fluid[1]. The entire system, including the cameras, is rotated in the same sense as the earth. Thus all observations are made relative to the solid-rotation rate, Ω, of the system, and they resemble observations of the earth made by geosynchronous satellites.

The cylindrical annulus experiments have some of the basic properties of the earth-atmosphere system, viz., a meridional thermal contrast called baroclinicity, and a non-Newtonian frame which is due to the solid rotation. Under laboratory conditions both these properties can be varied. Such variations have led to important results concerning the breakdown of toroidal (or Hadley) cells, the establishment of wave regimes -- which are asymmetric with respect to the axis of rotation -- and the re-establishment of the toroids[9].

It may be noted that the tropics are dominated by toroids (with a "weak" wave regime) and the extra-tropics by wave regimes[7]. Thus axially symmetric and asymmetric regimes coexist on the earth. This coexistence is due to the meridional variation of the local normal component of Ω. In the cylindrical annulus models the angular velocity Ω is *everywhere* normal to the base of the cylinders. Therefore these experiments do not possess an important characteristic of the earth-atmosphere system.

A spherical annulus model (see Fig. 1), which has meridional variations of temperature and the local

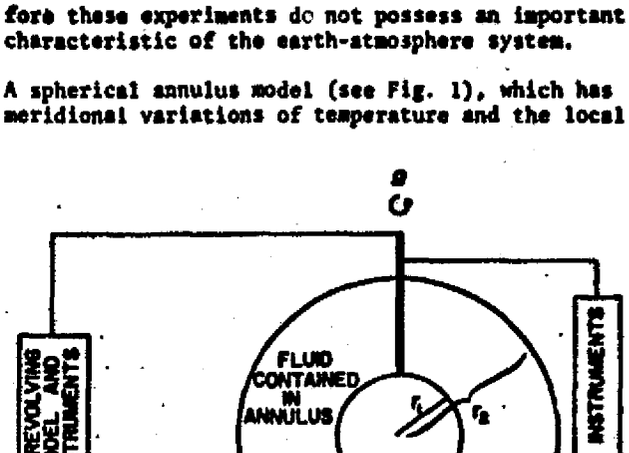

Fig. 1. The experimental setup for the zero-gravity, spherical atmospheric model.

normal component of Ω, cannot be used under normal earth gravity to simulate the behavior of the atmosphere. Such a model may be used successfully under very low or zero gravity conditions. It has been suggested that a zero-gravity, spherical model must have a radial gravitational field, simulated by the imposition of an electrical force[4] on the fluid. The consumption of electricity for this purpose, however, is a significant fraction of that available in a satellite[2]. Hence an alternative should be found. We suggest here that the inertia forces of the spherical annulus model may be used to simulate the effects of a radial gravitational field.

FORCES ACTING ON THE FLUID IN THE MODEL

It is well-known from the governing equations of meteorology [see, e.g., Haltiner[5], Holton[6]] that the forces to be considered in meteorology are i. the inertia forces due to the rotation of the coordinate system, viz. the centrifugal and Coriolis forces, ii. the pressure-gradient forces, iii. the buoyancy force, iv. the viscous forces and v. the gravitational force. Other kinds of forces are of negligible importance in meteorology.

We note that (static) atmospheric pressure is due to gravity. Thus pressure-gradient forces are indirectly due to gravity.

In Fig. 2 we present all the possible components of the inertia forces in a spherical coordinate system.

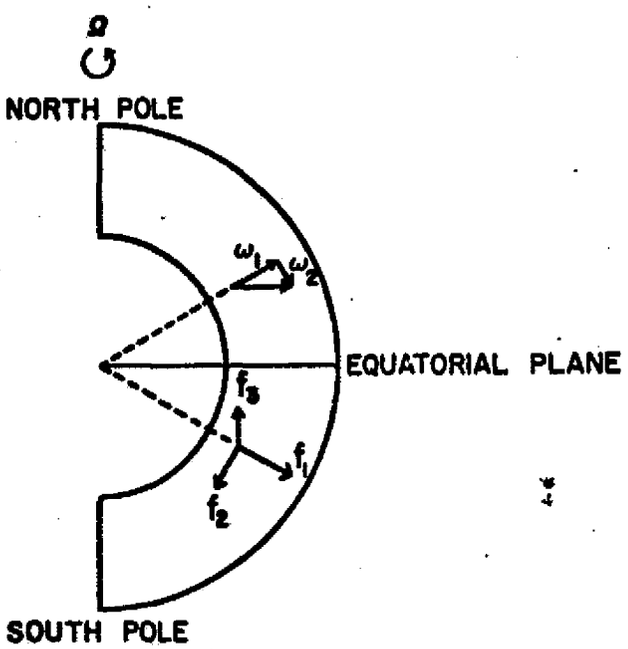

Fig. 2. The components of the inertia forces in the spherical model. The symbols are described by Eqs. 1 to 5.

These are represented mathematically as follows:

$$\omega_1 = r\Omega^2 \cos^2\phi, \quad \text{(radial centrifugal force)}, \tag{1}$$

$$\omega_2 = -r\Omega^2 \cos\phi \sin\phi, \quad \text{(north-south centrifugal force)}, \tag{2}$$

$$f_1 = 2\Omega u \cos\phi, \quad \text{(radial Coriolis force)}, \tag{3}$$

$$f_2 = -2\Omega u \sin\phi, \quad \text{(north-south Coriolis force)}, \tag{4}$$

and $f_3 = 2\Omega v \sin\phi - 2\Omega w \cos\phi$,
$f_{3,1}$ $f_{3,2}$
(east-west Coriolis force). (5)

In the above equations r is the radial distance from the common center of the two spheres in Fig. 2, Ω the angular velocity of the system, φ latitude angle, and u, v, w the eastward, northward and upward components of motion, respectively. The components of motion are positive if in the sense mentioned above.

The distributions of these forces clearly obey the following limiting conditions:

$$\omega_1, \omega_2, f_1, f_{3,2} \to 0, \text{ as } \phi \to \pm\frac{\pi}{2} \tag{6}$$

$$\omega_2, f_2, f_{3,1} \to 0, \text{ as } \phi \to 0 \tag{7}$$

Combining Eqs. 1 and 3 we obtain the radial inertia force equation:

$$g_M = r\Omega^2 \cos^2\phi + 2\Omega u \cos\phi \tag{8}$$

In Eq. 8 the left-hand side term is analogous to gravity and hence is denoted by g; the subscript M stands for "model". Let us determine the relative magnitudes of the two right-hand side terms of Eq. 8. The ratio of these two terms is:

$$\frac{2\Omega u \cos\phi}{r\Omega^2 \cos^2\phi} = \frac{2u}{\Omega r \cos\phi}. \tag{9}$$

The right-hand side (rhs) of Eq. 9 represents a Rossby number, denoted by Ro.

It is well known in meteorology that the condition for the prevalence of quasi-geostrophic equilibrium is that Ro << 1 [see, e.g., Holton [6]]. Since tropospheric motions are quasi-geostrophic, and since we want to reproduce and study such conditions in our model, we may assume that for our model experiments also Ro << 1. [The validity of this assumption can be experimentally established by making r_1 small. See Eq. 16 below.] Using this value in Eq. 9 we see that:

$$2\Omega u \cos\phi \ll r\Omega^2 \cos^2\phi. \tag{10}$$

Thus the second rhs term of Eq. 8 is negligible against the first rhs term. Therefore Eq. 8 reduces to:

$$g_M = r\Omega^2 \cos^2\phi. \tag{11}$$

Equation 11 may be interpreted as follows: In a spherical, inviscid, homogeneous, rotating fluid mass not acted on by gravitational forces, the radial centrifugal force acts as a spherically asymmetric gravity-like force.

CHARACTERISTIC PRESSURE DISTRIBUTION IN THE MODEL

The hydrostatic equation is:

$$\delta p = - g \rho \delta r, \qquad (12)$$

where $\delta p/\delta r$ is the variation of pressure with the (vertical) coordinate r, g the acceleration due to gravity, and ρ the density of the fluid. Let us assume, for the moment, that ρ is constant. Substituting Eq. 11 in Eq. 12, and integrating from r, the radial position at which the pressure is to be determined, to r_1, the radius of the inner sphere, we obtain:

$$p(r,\phi) = \frac{\rho}{2} \Omega^2 (r^2 - r_1^2) \cos^2\phi. \qquad (13)$$

From Eq. 13 it may be seen that the pressure due to the radial centrifugal force is a maximum at the outer sphere radius ($r = r_2$) at the equator ($\phi = 0$, $\cos \phi = 1$). The pressure diminishes to zero at both poles; it is also zero at the inner sphere (see Fig. 3).

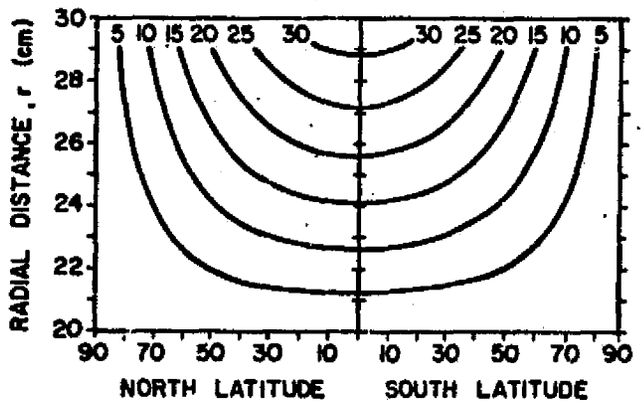

Fig. 3. The distribution of static pressure due to the radial centrifugal force in a spherical, zero-gravity model of the atmosphere. Units: dynes cm^{-2}.

DISTRIBUTION OF ZONAL MOTION DUE TO INERTIA FORCES

From Eq. 13 the equation for the north-south pressure-gradient force is obtained as

$$- \frac{1}{\rho} \frac{\partial p}{r \partial \phi} = \frac{\Omega^2}{r} (r^2 - r_1^2) \sin \phi \cos \phi. \qquad (14)$$

Combining this force with the other north-south inertia forces (Eqs. 2 and 4) we obtain

$$\frac{dv}{dt} = \frac{\Omega^2}{r} (r^2 - r_1^2) \sin \phi \cos \phi - r\Omega^2 \cos \phi \sin \phi - 2\Omega u \sin \phi. \qquad (15)$$

If the meridional acceleration $dv/dt = 0$, Eq. 15 yields

$$u = - \frac{\Omega}{2} \frac{r_1^2}{r} \cos \phi. \qquad (16)$$

The following points concerning Eq. 16 are worth noting:

i. At the equator ($\phi = 0$) every one of the rhs terms of Eq. 15 is zero. Thus u is indeterminate at the equator. Therefore, Eq. 16 is invalid in the vicinity of the equator, and the maximum magnitudes of the zonal motion due to inertia forces may be expected in the middle latitudes.

ii. In the above considerations, the effects of viscosity have not been taken into account. For any viscous fluid a no-slip condition has to be applied at the spherical walls. Hence the fluid in contact with the walls will have only the solid-rotation velocity.

iii. Since the easterlies represented by Eq. 16 are dissipated by viscosity at the walls, angular momentum balance in the model requires that westerlies be dissipated elsewhere. This might be expected to happen in the tropics, where viscous forces might help establish toroidal cells in the manner of Pearson[8].

iv. Since easterlies are established in the midlatitudes by the inertia forces in the spherical annulus model, it is essential that the model be heated in the equatorial regions, and cooled near the poles to produce westerlies in the midlatitudes, as in the earth's atmosphere. We also note from Eq. 16 that the easterlies established by inertia forces can be reduced by decreasing the value of r_1. If $r_1 = 0$ (i.e., for a spherical fluid mass), the zonal motion due to inertia forces is identically zero.

GENERATION OF THERMAL CONVECTION

It was shown earlier that the radial centrifugal force is much larger than the radial Coriolis force under quasi-geostrophic conditions, and that the radial centrifugal force is a function of radial distance r and latitude ϕ. When the radial centrifugal force is the dominant radial force, the warming of the equatorial regions near r_1, the inner radius, will not lead to thermal convection, since only denser fluid is drawn to the outer radius r_2. Therefore, to simulate cellular convection, the fluid must be heated at r_2 rather than at r_1. We note also the following: 1. Even if the entire outer sphere is heated, convection will not be generated at the poles, since the radial centrifugal force is zero at these points. 2. The heating of the outer sphere leads to a radial distribution of temperature in the model corresponding to the vertical (radial) distribution of potential temperature in the atmosphere. This is the proper similarity between the incompressible fluid in the model and the compressible atmosphere.

CONCLUSION

It can be readily shown that the meridional pressure gradient due to the radial centrifugal force (Eq. 14) leads to the establishment of westerlies which increase in magnitude radially, under geostrophic conditions. However, the meridional centrifugal force counteracts this, and establishes easterlies in the middle latitudes (see Eq. 16). Therefore the establishment of westerlies in the midlatitudes of the spherical annulus model demands the imposition of a meridional temperature gradient. It has been shown above that heating the outer sphere, rather than the inner sphere, leads to thermal convection under geostrophic conditions. If, however, zonal velocity u becomes comparable to Ωr, so that Ro $\sim$ 1 (see Eq. 9), the radial Coriolis force also becomes important in establishing thermal convection. Under such conditions the equations of motion are quite non-linear, and the resulting circulations have to be studied through actual experiments or through numerical models. We have begun a numerical model study at this time.

ACKNOWLEDGEMENTS

The author benefited much from stimulating discussions with Professor B. Haurwitz and Mr. J.P. McGuirk of the Department of Atmospheric Science, Colorado State University. The author is grateful to Professors C. Byron Winn and Elmar R. Reiter for enabling the performance of this research, and to Mr. Scott Ryden, Mrs. Ann Spahr and Mrs. Grace Holt for helping prepare this paper. This research was supported by the National Aeronautics and Space Administration, Marshall Space Flight Center, Huntsville, Alabama under Grant NAS 8-31347.

REFERENCES

(1) Douglas, M.A., R. Hide and P.J. Mason, "An investigation of the structure of baroclinic waves using three-level streak photography", QUART. J. ROY. METEOR. SOC., 98 (1972), 247-263.

(2) Fichtl, George, NASA - Marshall Space Flight Center, Huntsville, Alabama. Personal communication (1976).

(3) Fultz, D., R. Long, G. Owens, W. Bohan, R. Kaylor and J. Weil, "Studies of thermal convection in a rotating cylinder with some implications for large scale atmospheric motion", METEOROL. MONOGR., 4 (1959), 104 pp.

(4) Gilman, Peter A., High Altitude Observatory, NCAR, Boulder, Colorado. Personal communication (1975).

(5) Haltiner, G.J., "Numerical Weather Prediction", Wiley, New York (1971), 317 pp.

(6) Holton, J.R., "An Introduction to Dynamic Meteorology", Academic Press, New York (1972), 319 pp.

(7) Oort, Abraham H. and Eugene M. Rasmusson, "Atmospheric Circulation Statistics", NOAA Professional Paper 5, U.S. Dept. of Commerce, Rockville, Md. (1971), 323 pp.

(8) Pearson, C.E., "A numerical study of the time-dependent viscous flow between two rotating spheres", J. FLUID MECH., 28 (1967), 323-336.

(9) Quinet, A., "A Numerical Study of Vacillation", ADVANCES IN GEOPHYS., 17, Academic Press, New York (1974), 101-186.

Reprinted from JOURNAL OF THE ATMOSPHERIC SCIENCES, Vol. 33, No. 10, October 1976
American Meteorological Society
Printed in U. S. A.

Two Similarities Between Atmospheric Eddies and Linear Baroclinic Waves

S. SRIVATSANGAM

Department of Atmospheric Science, Colorado State University, Fort Collins 80523

(Manuscript received 18 May 1976, in revised form 18 June 1976)

ABSTRACT

Very good agreement is shown to exist between the meridional distributions of the zonal wavenumber n of rapidly amplifying baroclinic waves on a sphere and of an average wavenumber $\bar{n}$ of "grid-scale" atmospheric eddies. As a consequence, the zonal wavelength of both baroclinic and atmospheric eddies remains virtually constant, i.e., within a factor of 2, over the extratropics. The values of n at different latitudes have been obtained by using linearized baroclinic theory on different meridional profiles of the unperturbed zonal wind (MPUZW). Since they agree with $\bar{n}$, atmospheric eddies are, in relation to linear baroclinic waves, independent of MPUZW. In this sense $\bar{n}$ is controlled locally rather than globally.

The mutual dependence of the upward and poleward transports of (sensible) heat in baroclinic wave theory is correctly formulated—as compared to a direct analysis of the first law of thermodynamics.

1. Introduction

Moura and Stone (1976, hereafter referred to as M & S) and Stone (1974) have derived a number of interesting properties of linear baroclinic waves. They have compared their results with available meteorological statistics such as those of Oort and Rasmusson (1971) and found quite good agreement. In the case of two specific results, additional methods can be used to infer the properties of atmospheric eddies, which may then be compared with the M & S results. The methods we have alluded to will be discussed in this paper. The results under consideration are the zonal scale of eddies and the interdependence of the poleward and upward transports of heat.

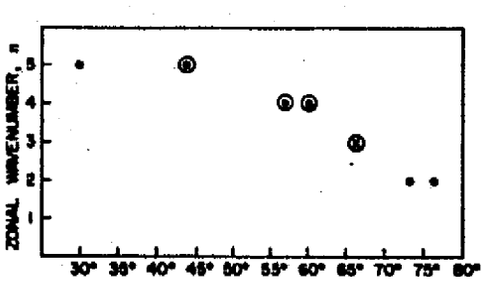

FIG. 1. The latitude dependence of zonal wavenumber for linear baroclinic waves on a sphere: dots, near-neutral stability (symmetric streamfunction); circled dots, far from neutral stability (symmetric streamfunction); circled cross, far from neutral stability (streamfunction antisymmetric with respect to the equator). Abscissas of points refer to the latitudes at which the geopotential eigenfunction, at the top level of the three-level model of Moura and Stone (1976), reaches the maximum magnitude. Each point corresponds to a different meridional profile of the unperturbed zonal wind.

2. The zonal scale of eddies

For the study of this property we consider the spherical, two-layer (three-level), linear quasi-geostrophic model of M & S. M & S use several meridional profiles of the unperturbed zonal wind (MPUZW). Their results concerning the zonal scale of linear baroclinic waves may be summarized as follows:

1) The nearer the peak in perturbation geopotential is to the pole, the smaller is the zonal wavenumber (n) of the most unstable mode (see Fig. 1).

2) As a consequence of 1), the zonal wavelength near the peak in perturbation geopotential is about 5000 km on a sphere of the size of the earth. (This wavelength is virtually independent of latitude in a broad midlatitude belt.)

3) The zonal wavelength is proportional to the radius of deformation at the latitude where the maximum of perturbation geopotential occurs.

The author (Srivatsangam, 1976a, b) has described a parametric method which yields an average zonal wavenumber $\bar{n}$ for atmospheric eddies through the geostrophic meridional wind equation. Here, the overbar denotes a weighted root-mean-square averaging (for details, see Srivatsangam, *op. cit.*) Now,

$$\bar{n} = ([v^{*2}]/[s^{*2}])^{\frac{1}{2}}(g^{-1}fa\cos\phi), \qquad (1)$$

where square brackets denote zonal averages and asterisks departures therefrom. Hence $[v^{*2}]$, $[s^{*2}]$ represent the zonal variances of the geostrophic meridional wind at, and the height of, an isobaric surface, respectively. Also, f is the Coriolis parameter, a the mean radius of the earth, ϕ latitude, and g the

TABLE 1. Height and latitude variations of the monthly mean values $M(\hat{n})$ and the temporal coefficient of variation $C(\hat{n})$ of the average zonal wavenumber $(\hat{n})$.

Pressure (mb)	Latitude (°N) 20	25	30	35	40	45	50	55	60	65	70	75	80	85
						a. $M(\hat{n})$ for October 1968								
100	4.02	3.81	3.77	3.87	4.10	3.92	3.29	2.70	2.25	1.86	1.59	1.39	1.27	1.11
200	4.23	4.26	4.48	4.71	4.83	4.57	4.03	3.47	2.93	2.41	2.05	1.79	1.49	1.25
300	5.13	4.88	4.95	5.16	5.10	4.76	4.27	3.77	3.25	2.72	2.36	1.98	1.62	1.32
500	5.61	5.31	5.26	5.44	5.03	4.64	4.20	3.62	3.11	2.63	2.27	1.89	1.61	1.27
700	5.05	5.17	5.24	5.14	4.84	4.53	4.03	3.49	3.07	2.63	2.21	1.88	1.61	1.24
1000	4.95	4.98	5.26	5.38	5.16	4.68	4.08	3.63	3.35	3.07	2.70	2.09	1.55	1.14
						b. $C(\hat{n})$ for October 1968								
100	20	15	12	11	11	15	15	20	26	21	21	19	19	14
200	17	15	14	13	12	15	16	17	21	19	21	26	20	25
300	12	13	14	12	13	15	17	17	18	17	24	22	19	21
500	9	11	13	10	12	16	17	17	17	17	25	20	19	19
700	14	12	10	9	10	15	16	16	16	18	20	23	25	18
1000	20	19	14	13	12	14	14	17	19	16	19	21	21	14
						c. $M(\hat{n})$ for February 1969								
100	3.29	3.36	3.71	4.02	3.60	2.93	2.48	2.20	2.02	1.94	1.86	1.59	1.34	1.15
200	3.46	3.77	4.45	4.94	4.61	3.62	3.03	2.67	2.41	2.37	2.45	2.16	1.43	1.09
300	4.13	4.43	5.07	5.15	4.88	3.86	3.30	3.02	2.77	2.71	2.73	2.23	1.51	1.15
500	4.60	4.73	4.88	4.92	4.74	3.79	3.36	3.18	2.94	2.84	2.81	2.14	1.50	1.18
700	4.88	4.67	4.86	4.81	4.63	3.91	3.43	3.23	3.04	2.93	2.66	2.05	1.52	1.18
1000	5.01	4.93	5.54	5.37	4.46	3.67	3.21	3.05	2.96	2.70	2.59	2.14	1.63	1.27
						d. $C(\hat{n})$ for February 1969								
100	11	10	15	19	13	14	18	17	14	15	17	20	21	18
200	13	10	10	11	16	11	18	20	15	12	17	25	19	6
300	17	14	11	11	16	12	19	23	16	14	15	22	19	11
500	16	12	13	13	17	14	20	23	18	15	14	21	19	14
700	15	13	18	16	15	11	17	22	21	17	13	22	24	14
1000	11	12	16	17	15	15	20	23	26	20	22	24	23	22

acceleration due to earth's gravity. From (1) it is seen at once that $\hat{n}$ represents "grid-scale" atmospheric eddies.

The daily values of $\hat{n}$ were computed at the 100, 200, 300, 500, 700 and 1000 mb levels in the region 20°N to 85°N using the National Meteorological Center (NMC) data for October through December, 1968, and February through April, 1969. The hour of observation of the data used here was 1200 GMT, and a 5° latitude by 5° longitude grid was used.

The data on monthly mean values of $\hat{n}$, denoted by $M(\hat{n})$, are presented in Table 1. These are for October 1968 and February 1969 only, but are typical of all the six months for which computations were made.

From Table 1 and Fig. 1 it is readily seen that result 1), and hence result 2), of M & S are in good agreement with the ensemble characteristics of atmospheric eddies as represented by $\hat{n}$.

It may be repeated here that each data point in Fig. 1 corresponds to a *different* MPUZW. However, the data of Fig. 1 and Table 1 show excellent correspondence. From these, the following conclusions may be made:

In order to derive the typical wavenumber of atmospheric eddies in any particular latitude through linear baroclinic wave theory, a MPUZW which would yield a maximum value of perturbation geopotential height at that latitude must be used.

Conversely, the zonal wavenumber of atmospheric eddies at each latitude is such as if the maximum magnitude of perturbation geopotential height occurs at that latitude.

Also, from the last statement and result 3) of M & S, it follows that the zonal wavelength of atmospheric eddies is proportional to the radius of deformation at each latitude. [This does not contradict result 2) of M & S. Since the radius of deformation is proportional to $1/f$, which varies by a factor of 2 from 30°N to 90°N, the typical wavelength of linear baroclinic and atmospheric eddies varies only by a factor of 2 in the extratropics. On the other hand, the wavenumber, as seen from Table 1, varies by a factor of 5 from the subtropics to the subpolar region. By comparison, therefore, the wavelength rather than the wavenumber is constant across latitude circles.]

Now we turn to the question of the temporal variability of $\hat{n}$. Table 1 contains data on the temporal co-

TABLE 2. Height and latitude variations of the temporal coefficients of variation $C([z^{*2}])$ and $C([v^{*2}])$ of the zonal variances of isobaric surface height and geostrophic meridional wind.

Pressure (mb)	Latitude (°N) 20	25	30	35	40	45	50	55	60	65	70	75	80	85
a. $C([z^{*2}])$ for October 1968														
100	35	33	28	28	29	31	34	51	66	75	81	84	88	93
200	37	32	32	39	35	24	24	33	41	51	64	73	86	111
300	36	32	37	49	38	25	24	25	31	43	56	69	86	116
500	31	33	45	56	39	31	29	23	29	45	51	67	83	108
700	35	31	32	39	42	39	31	24	27	46	48	65	93	119
1000	44	29	35	22	51	57	33	31	33	34	41	57	91	99
b. $C([v^{*2}])$ for October 1968														
100	38	30	20	34	40	31	30	36	42	51	62	67	73	86
200	27	31	27	41	41	25	32	36	29	35	51	56	63	93
300	30	34	35	46	44	25	31	33	27	37	48	52	61	93
500	30	33	38	45	39	26	33	35	30	42	45	52	62	86
700	35	31	27	35	38	31	35	37	29	41	39	45	69	99
1000	44	35	36	33	46	48	41	43	35	29	34	36	60	90

efficient of variation of $\hat{n}$ given by

$$C(\hat{n}) = \frac{\sigma(\hat{n})}{M(\hat{n})} \times 100, \qquad (2)$$

where $\sigma(\hat{n})$ is the monthly standard deviation of $\hat{n}$. Using the data described above, $C(\hat{n})$ was calculated for all latitudes, pressure levels and months.

The $C(\hat{n})$ data in Table 1 indicate rather small day-to-day variations in $\hat{n}$. A comparison of the coefficients of variation of $[v^{*2}]$, $[z^{*2}]$ (see Table 2) and $\hat{n}$ shows that $C(\hat{n})$ is only about one-half as large as $C([z^{*2}])$ and $C([v^{*2}])$. From (1), then, it follows that variations in $[z^{*2}]$ are compensated by like variations in $[v^{*2}]$. This is confirmed by Fig. 2, in which the daily values of $[z^{*2}]$, $[v^{*2}]$ and $\hat{n}$ for 65°N, 200 mb and October 1968 are presented.

The temporal quasi-constancy of $\hat{n}$ thus achieved by the mutual compensation of $[z^{*2}]$ and $[v^{*2}]$ indicates that the results of M & S are valid not only on a monthly mean basis, but also on a daily basis, i.e., for transient atmospheric states.

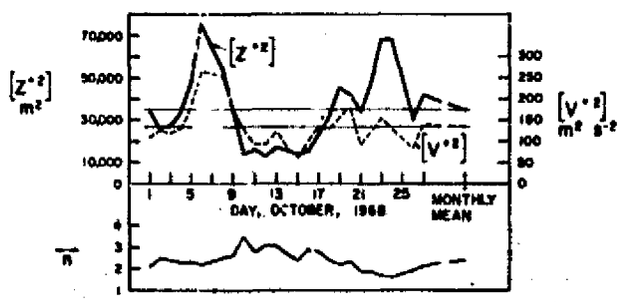

FIG. 2. Daily values of the zonal variances of the geostrophic meridional wind $[v^{*2}]$ and the height of the 200 mb surface $[z^{*2}]$, and the weighted root-mean-square wavenumber $\hat{n}$. Values are for 200 mb, 65°N and October 1968.

Finally, the $M(\hat{n})$ values for October 1968 and February 1969 in Table 1 reveal rather small inter-monthly changes. This is also true of the other months for which computations were made. Thus it appears that in each zone $\hat{n}$ remains nearly constant at least through the cold half of the year. This may be compared with the phenomenon of vacillation in the cylindrical annulus experiments (see, e.g., Lorenz, 1963, and Pfeffer and Chiang, 1967). Vacillation is a process in which, under constant conditions of rotation and imposed radial thermal gradient, the wavenumber remains a constant whereas the wave amplitude or radial axis tilt varies cyclically in time. Since $\hat{n}$ remains nearly constant in the atmosphere, a similar ensemble average wavenumber may perhaps also remain constant in unsteady Rossby regimes. These arguments are, however, quite conjectural, and need verification through data analyses.

3. The interdependence of vertical and meridional eddy heat fluxes

Stone (1974) has derived the following equation for the upward flux of the sum of sensible heat plus potential energy [which may be closely approximated by the upward flux of sensible heat (see Oort and Rasmusson, 1971, pp. 50–51)]:

$$[\theta^* w^*] = -2nc_i|x^*_3 - x^*_1|^2 + 2[u][\theta^* v^*]. \qquad (3)$$

In (3), θ^* is perturbation potential temperature, u, v, w the zonal, meridional and vertical components of velocity, respectively, x^*_3, x^*_1 the *amplitude* of perturbation pressure at the top and bottom levels, respectively, and c_i the imaginary part of the complex phase speed. Eq. (3) applies to baroclinic waves on a β plane. Since $c_i \approx 0$ near neutral stability, $[\theta^* w^*]$ is directly proportional to $[\theta^* v^*]$. M & S have extended this result

of Stone (1974) to baroclinic states far from neutral stability, and on a sphere, and concluded that even for these cases $[\theta^* w^*]$ is proportional to $[\theta^* v^*]$. Therefore, the first right-hand side term of (3) is negligible as compared to the second.

Kuo (1956), examining baroclinic instability in a cylindrical coordinate system, has derived equations similar to (3) above [Kuo, *op. cit.*; Eqs. (72) and (73)]. The numerical values given by Kuo for the upward flux of sensible heat are in order-of-magnitude agreement with meteorological observations.

Srivatsangam (1976a) has derived the following equation for the upward flux of sensible heat, from the first law of thermodynamics:

$$\begin{aligned} c_p[\rho][w^*T^*] &= -[\rho]c_p\{\Gamma_d^{-1}\{\partial[T^{*2}]/2\partial t+[v](\partial[T^{*2}]/2a\partial\phi) \\ &\quad +[w](\partial[T^{*2}]/2\partial\xi)+[v^*T^*]\partial[T]/a\partial\phi\} \\ &\quad +k^{-1}\{[T^*\partial q^*/\partial t]+[u][T^*\partial q^*/a\cos\phi\partial\lambda] \\ &\quad +[v][T^*\partial q^*/a\partial\phi]+[w][T^*\partial q^*/\partial\xi] \\ &\quad +[v^*T^*](\partial[q]/a\partial\phi)\}\}\div(1+\gamma). \end{aligned} \quad (4)$$

In (4), c_p is specific heat of air at constant pressure, ρ air density, T temperature, Γ_d the dry adiabatic lapse rate, $k=g/L$, L being the latent heat of vaporization of water, q the specific humidity of air, ϕ, λ, ξ and t latitude, longitude, altitude and time, respectively, and

$$\gamma=\Gamma_d^{-1}\partial[T]/\partial\xi+k^{-1}\partial[q]/\partial\xi.$$

Eq. (4) involves several assumptions including the omission of diabatic effects other than the release of latent heat of vaporization of water and the negligibility of triple correlation terms such as $[T^*v^*\partial T^*/a\partial\phi]$.

We see that only two terms on the right-hand side of (4) involve the factor $[v^*T^*]$. An order-of-magnitude estimate of all right-hand side terms of (4), using the Oort and Rasmusson (1971) data as reference, shows that the term involving $[v^*T^*]\partial[T]/a\partial\phi$ is at least one order of magnitude larger than the other terms. Thus the formulation of the interdependence between upward and poleward fluxes of sensible heat in baroclinic wave theory is in agreement with a direct analysis of the first law of thermodynamics. However, very many other effects are neglected in deriving an equation like (3), although these effects are small. Thus, order-of-magnitude agreement between the predictions of linear baroclinic wave theory and meteorological data may be expected even in the case of upward eddy heat flux. This is indeed proved by the results of Kuo, mentioned above.

Acknowledgments. The author wishes to thank Mrs. Susan Kuehl for typing this manuscript. This research was sponsored in part by the National Aeronautics and Space Administration- Marshall Space Flight Center, under Grant NAS 8-31347 and in part by the U. S. Navy Environmental Prediction Research Facility, under Grant N 00228-76-C-3205.

REFERENCES

Kuo, H.-L., 1956: Energy-releasing processes and stability of thermally driven motions in a rotating fluid. *J. Meteor.*, 13, 82–101.

Lorenz, E. N., 1963: The mechanics of vacillation. *J. Atmos. Sci.*, 20, 448–464.

Moura, A. D., and P. H. Stone, 1976: The effects of spherical geometry on baroclinic instability. *J. Atmos. Sci.*, 33, 602–616.

Oort, A. H., and E. M. Rasmusson, 1971: Atmospheric circulation statistics. NOAA Prof. Pap. 5, 323 pp. [Available from U. S. Govt. Printing Office, Stock No. 0317-0045, C 55.75:5.]

Pfeffer, R. L., and Y. Chiang, 1967: Two kinds of vacillation in rotating laboratory experiments. *Mon. Wea. Rev.*, 95, 75–82.

Srivatsangam, S., 1976a: Atmospheric eddy transports and their efficiencies. Ph.D. dissertation, Colorado State University, 87 pp. [Also available as Environ. Res. Pap. No. 3, Dept. Atmos. Sci. Colorado State University.]

——, 1976b: A problem in the parameterization of large-scale eddies. *Tellus*, 28, No. 3, 193–196.

Stone, P. H., 1974: The meridional variation of eddy heat fluxes by baroclinic waves and their parameterization. *J. Atmos. Sci.*, 31, 444–456.